Track Constrained RTK-like Positioning for Railway Applications

ALESSANDRO NERI
University of Roma TRE, Rome, Italy

ROBERTO CAPUA
SOGEI, Rome, Italy

PIETRO SALVATORI
RADIOLABS, Rome, Italy

Received May 2017; Revised May 2018

ABSTRACT: *Here, we investigate PVT solutions based on multi-constellation receivers and dedicated augmentation networks allowing to determine the track on which a train is operating with a very high safety Integrity level. Because the time needed to accomplish this task has a relevant impact on the rail traffic management performance and, therefore, it is considered a key performance indicator by rail infrastructure managers, a double frequency solution is investigated. Particularly, we focus our attention on the advantages of relative positioning solutions, based on Double-Difference Wide-Laning Carrier Phase measurement combination, exploiting the fact that the train location is completely determined by its mileage due to the track constraint, to speed up track discrimination. No ambiguity fix is required at this scope. Here, a detailed description of the overall processing and achievable performance is given. Performance assessment is provided by means of Monte Carlo simulations based on observations recorded on field campaigns.* © *2018 The Authors. Navigation published by Wiley Periodicals, Inc. on behalf of Institute of Navigation.*

INTRODUCTION

Integration of GNSS technologies into modern train control systems may produce a yearly rate of railway market expansion 1.5 times higher than the one that would have been derived by the adoption of traditional track-side technology. The cost saving has particular impact on the regional/local lines for which current location technologies, based on transponders, named balises, installed along the tracks at georeferenced sites, are not economically sustainable. This fact has motivated the adoption by the European Union Agency for Railways (formerly European Railways Agency) of the EGNSS (European Global Navigation Satellite Systems) assets into the European Rail Train Management System (ERTMS) Train Control System (TCS) platform [1].

However, GNSS-based train location determination solutions will succeed in replacing the current technologies based on balises and track circuits if, and only if, it will be cost-effective. To this end, recently both ESA (European Space Agency) and GSA (European GNSS Agency) fostered several projects (e.g., 3Insat, ERSAT EAV, RHINOS, and STARS) aimed at the development and certification of solutions compliant with the next release of the ERTMS standard incorporating GNSS technologies.

Considering that during normal operational conditions, track-side equipment foreseen by ERTMS (Level 2), like track circuits, allows for determination of which track the train lies on, the attention of scientists and manufacturers has been focused on the task of determining the current train mileage (in mathematical terms, the curvilinear coordinate) with respect to the known track.

The main challenge, in this case, is to provide a cost-effective solution compliant with the severe rail integrity requirements asking for a Tolerable Hazard Rate not exceeding 10E-9 Hazard/h, at

[Correction added on 10 November, after first online publication: Grammatical and formatting changes have been made to the article to improve clarity.]

NAVIGATION: *Journal of The Institute of Navigation*
Vol. 65, No. 3, Fall 2018
Printed in the U.S.A.

system level. The outcomes of those projects indicate that adoption of multi-constellation receivers and next generation Wide Area Augmentation Systems, like the American WAAS and the European EGNOS, should guarantee the medium accuracy necessary for an effective and safe control of train traffic, when the train itinerary (i.e., the ordered sequence of tracks) is known by other means [1–3].

However, cases in which it is not possible to determine, with an acceptable confidence level, the starting track occupied by the train, by means of the current track side equipment still exists. For this reason, at the start of missions, trains have to run in Staff Responsible Mode (SRM) until the first group of transpoders (eurobalises) is met and its identity is verified by the Control Center (i.e., the Radio Block Center).

Since SRM implies very low average speeds (e.g., $<$40 km/h) and very low accelerations, this fact produces a waste of time, and then money, every time a service starts. Thus, rail infrastructure managers (like RFI in Italy) are starting to ask for GNSS-based solutions able to determine the track occupied by the train without the need for installing physical balises.

As observed in [4], track discrimination based on code pseudoranges that do not explicitly account for the track constraint may exhibit very poor performance. Although PVT algorithms that impose the track constraint and make use of multiple independent measures at different epochs for improving performance can be designed, the time needed to guarantee the required Integrity is of major concern.

The train moving on the track is characterized by a harsh environment (multipath, foliage, shadowing, high dynamics). While for RTK positioning, standard Carrier Phase Ambiguity Decorrelation techniques can be used for fast high precision solutions [5–10], the time needed for the On-Board Unit (OBU) for fixing integer ambiguities and the relevant portion of floating solutions [11–13] leads to the need for the investigation of alternative PVT means without ambiguity fixing.

Thus, in this paper, we investigate an innovative PVT solution based on multi-constellation receivers and dedicated augmentation networks that allow determination of the unknown track at the start of mission with the required integrity in a very short time. In particular, we focus our attention on relative positioning, based on Double-Difference Wide-Laning Carrier Phase measurement combination that benefits from the constraint represented by the track for the train location, in order to speed up track discrimination. No ambiguity fix is required at this point.

In this contribution, a detailed description of the overall processing and achievable performance is given. Assessment of the performance is provided by means of Monte Carlo simulations making use of observations recorded in the framework of the European Union Horizon 2020 Galileo-2014-1 ERSAT EAV Project.

A TRACK DISCRIMINATION METHOD BASED ON HYPOTHESIS TESTING

In the presence of multiple tracks, PVT estimation can be formulated as a combination of hypothesis testing (i.e., which is the current track in use by the train) and parameter estimation (i.e., given a track, what is the train mileage?). However, the mileage of a train can be considered an unknown random parameter, similarly to what happens in the radar detection of targets whose range and velocity are unknown. In this case, as suggested in [14, 15], we can apply the *generalized likelihood ratio test*, as defined in [16].

Therefore, assuming that the train can be located along one of M tracks and considering the kth hypothesis as corresponding to the kth track, extending the approach proposed in [4, 17, 18] by the authors for code processing,

- We first estimate, for each candidate track, and for each phase ambiguity set, the curvilinear abscissa of the receiver by means of a weighted least square estimator (WLSE), assuming that the corresponding hypothesis is true.
- We then use these conditional estimates to compute the measurement residuals associated with each hypothesis and, from them, the likelihood of each track.

Those likelihoods are then combined in generalized log-likelihood ratio tests to detect the current track. In fact, assuming that the hypotheses are uniformly distributed, the track detection rule selects the hypothesis corresponding to the largest of them.

Moreover, multiple observations can be combined as in [4]. Since the generalized log-likelihood ratio magnitudes provide information about the reliability of the decision, their values are compared with thresholds to verify that enough information has been acquired before a decision on which track the train is lying is made.

For each track, the PVT estimate is computed by solving a set of nonlinear equations relating the observables (e.g., pseudoranges and carrier phases) to the train mileage and phase ambiguities by means of an iterative procedure, accounting for the different statistics of the equivalent measurement noise due to both satellite elevation and signal characteristics specific to each constellation.

In the next sections, a detailed description of the overall processing and achievable performance is given.

The ERTMS Safety Integrity requirements ask for a rate of deciding the wrong track to be lower than 10E-9 error/h. To understand the impact of such a requirement on the accuracy of the GNSS-based train location determination system, when no other means for track discrimination are employed, let us examine first, the suboptimal solution that decides on which track the train is lying. We first compute the receiver location without imposing any track constraint and then search for the track nearest to the estimated train position.

As illustrated in Figure 1, in this case, a wrong decision is taken as soon as the position error component in the across-track direction exceeds half the inter-distance W between tracks, and no timely warning is provided. This means that, in this case, the Alert Limit AL equals $W/2$. Considering that the inter-distance W is just a few meters (e.g., 3 m), and assuming that one independent decision is taken every second, a standard deviation of the Gaussian distribution over-bounding the across-track position error component distribution of about 20 cm would be needed.

This requirement can be partially mitigated by combining the decisions based on two or more different constellations (e.g., GPS and GALILEO) by means of an N out of N (*NooN*) logic. In fact, in this case, a wrong decision is made only when all decisions are wrong and coincident. Thus, the probability that an *NooN* system will provide a wrong decision is bounded by the product of the discrimination error probabilities of the single-constellation detectors.

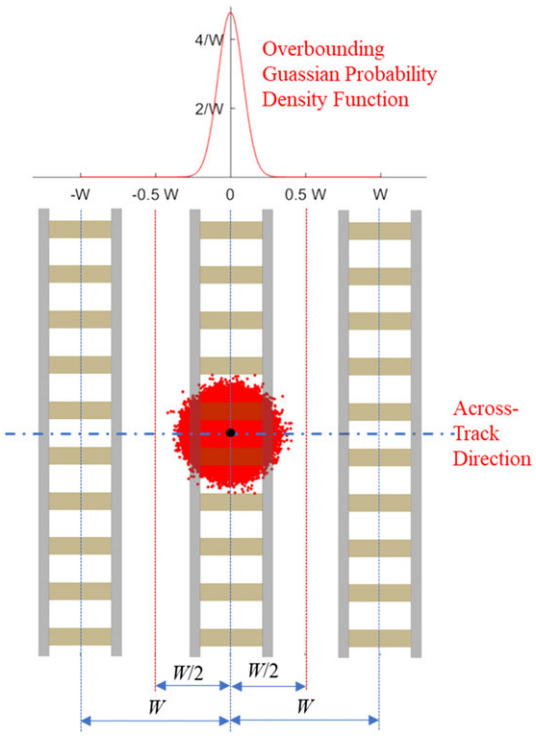

Fig. 1–Parallel track discrimination. [Color figure can be viewed at wileyonlinelibrary.com and www.ion.org]

Therefore, an overall track discrimination error rate of 10^{-9} error/h can be obtained by combining, with a 2*oo*2 logic, the outputs of two independent discriminators, using different constellations, having a discrimination error rate of 3.3×10^{-5} error/h. This in turn implies that, for an inter-distance W = 3 m, the standard deviation of the over-bounding Gaussian distribution should not exceed about 30 cm. Let us observe that when one of the two decisions is wrong, the 2*oo*2 logic will set the decision as unavailable. Considering that the probability of this event is given by the sum of the error probabilities of the two detectors minus their product, the rate of the decision unavailable event is 6.6×10^{-5} event/h. Then, based on that and considering that the actual procedure for the Start of Mission based on the physical balises has a duration of tens of seconds, the increment by one epoch (e.g., 1 s if the receiver is operating at 1 Hz) of the additional latency in GNSS-based track discrimination due to the unavailability is completely negligible.

TRACK CONSTRAINED DOUBLE-DIFFERENCE PVT EQUATIONS

To shorten the time needed to provide a decision about the train's track, in the following, we analyze the case of a two frequency receiver. Since centimeter accuracy is not requested, to avoid the risk of time propagation of wrong decisions caused by local hazards, like multipath, we focus our attention on memoryless solutions, separately processing the Signal In Space of each epoch. Thus, Kalman filtering is not employed.

Since the train is constrained to stay on track, at the kth epoch, the location of the OBU receiver $\mathbf{X}^{Train}(k)$ is completely determined by the knowledge of its curvilinear abscissa $s(k)$, referred in the following as train *mileage*, defined on the georeferenced railway track. Then, given the mileage $s(k)$, the Cartesian coordinates of the location of the receiver are described by the parametric equation:

$$\mathbf{X}^{Train}(k) = \mathbf{X}^{Train}[s(k)]. \tag{1}$$

As detailed in Appendix A, truncating to the first order, the Taylor series expansion of the geometric range equations around the point $\mathbf{X}^{Train}\left[\hat{s}^0(k)\right]$, corresponding to the initial guess $\hat{s}^0(k)$ of the train location, leads to the following double-difference measurement equations

$$\begin{bmatrix}\nabla\Delta\mathbf{P}_1\\ \nabla\Delta\mathbf{P}_2\\ \nabla\Delta\mathbf{L}_1\\ \nabla\Delta\mathbf{L}_2\end{bmatrix}-\begin{bmatrix}\nabla\Delta\mathbf{r}(\hat{s}^0)\\ \nabla\Delta\mathbf{r}(\hat{s}^0)\\ \nabla\Delta\mathbf{r}(\hat{s}^0)\\ \nabla\Delta\mathbf{r}(\hat{s}^0)\end{bmatrix}-\begin{bmatrix}\nabla\Delta\hat{\boldsymbol{\beta}}_1^P+c\nabla\Delta\hat{\mathbf{I}}_1+c\nabla\Delta\hat{\mathbf{T}}\\ \nabla\Delta\hat{\boldsymbol{\beta}}_2^P+c\nabla\Delta\hat{\mathbf{I}}_2+c\nabla\Delta\hat{\mathbf{T}}\\ \nabla\Delta\hat{\boldsymbol{\beta}}_1^\phi-c\nabla\Delta\hat{\mathbf{I}}_1+c\nabla\Delta\hat{\mathbf{T}}\\ \nabla\Delta\hat{\boldsymbol{\beta}}_2^\phi-c\nabla\Delta\hat{\mathbf{I}}_2+c\nabla\Delta\hat{\mathbf{T}}\end{bmatrix}=$$
$$=\begin{bmatrix}\mathbf{HG}(\hat{s}^0) & 0 & 0\\ \mathbf{HG}(\hat{s}^0) & 0 & 0\\ \mathbf{HG}(\hat{s}^0) & \lambda_1\mathbf{I} & 0\\ \mathbf{HG}(\hat{s}^0) & 0 & \lambda_2\mathbf{I}\end{bmatrix}\begin{bmatrix}\Delta s\\ \nabla\Delta\mathbf{N}_1^\phi\\ \nabla\Delta\mathbf{N}_2^\phi\end{bmatrix}+\begin{bmatrix}\nabla\Delta\mathbf{n}_1^P\\ \nabla\Delta\mathbf{n}_2^P\\ \lambda_1\nabla\Delta\mathbf{n}_1^\phi\\ \lambda_2\nabla\Delta\mathbf{n}_2^\phi\end{bmatrix}, \tag{2}$$

where

- $\nabla\Delta\mathbf{P}_i$ and $\nabla\Delta\mathbf{L}_i=\lambda_i\nabla\Delta\boldsymbol{\phi}_i$ are the column arrays of the double differences of the code and carrier phase pseudoranges expressed in meters, at frequency f_i;
- $\nabla\Delta\mathbf{r}(\hat{s}^0)$ are the column arrays of the double differences of the geometric distances of the satellites from the Master Station (MS) receiver and from the point $\mathbf{X}^{Train}[\hat{s}^0(k)]$ computed on the basis of the best available models for the satellite position;
- $\Delta s=s-\hat{s}^0$ is the incremental mileage of the train with respect to $\hat{s}^0$;
- $\mathbf{H}$ is the observation matrix of the ordinary (i.e., unconstrained) double-difference equations, given by (A-17);
- $\mathbf{G}(\hat{s}^0)$ is the unit vector of the along-track direction at the mileage $\hat{s}^0$:

$$\mathbf{G}(\hat{s}^0)=\left[\frac{\partial\mathbf{X}^{Train}}{\partial s}\right]_{s=\hat{s}^0}; \tag{3}$$

- $\nabla\Delta\mathbf{N}_i^\phi$ are the double differences of the carrier phase offsets (in multiples of the wavelength) at frequency f_i;
- $\nabla\Delta\mathbf{n}_i^P$ and $\nabla\Delta\mathbf{n}_i^\phi$ are the double differences of the errors of the time of arrival estimation algorithm, generated by multipath, GNSS receiver thermal noise, and eventual radio frequency interference, respectively, at the *MS* and the OBU GNSS receiver, modeled as Gaussian Random processes with covariance matrices given by (A-20);
- $\nabla\Delta\hat{\boldsymbol{\beta}}_i^P$ and $\nabla\Delta\hat{\boldsymbol{\beta}}_i^\phi$ are the estimates of the double differences of the biases, accounting for differences in latency and delay among channels, at both sides, satellite and receiver, as well as the wind-up effect and antenna phase center positions; and
- $\nabla\Delta\hat{\mathbf{I}}_i$ and $\nabla\Delta\hat{\mathbf{T}}$ are the estimates of the double differences of the ionospheric and tropospheric delays estimated from the best available models.

At the first epoch, $\hat{s}^0(k)$ can be set equal to the mileage of the track's point nearest the reference station. Then, the estimate at the previous epoch can be used.

In principle, since $\nabla\Delta\mathbf{N}_i^\phi$, representing the double differences of the initial phase ambiguities, are integer numbers, we could resort to the LAMBDA method, [5], and its variants, [6, 7], to solve (2). On the other hand, the probability of successfully fixing the ambiguities decreases with the increase of their number. Therefore, several methods to select the subset to fix have been proposed [8], including those trying to fix only the Wide Lane (WL) ambiguities [9, 10].

Although the track detector proposed here does not need to fix ambiguities, its complexity still depends on the number of different hypotheses concerning the initial phase ambiguity double differences for which the *a posteriori* probability has to be computed. Thus, as a trade-off between computational complexity and position accuracy, considering that in ERTMS, a centimeter accuracy is not required, we resort here to the use of the Wide Lane (WL) combination $\nabla\Delta\mathbf{L}_{WL}$ [19], with

$$\nabla\Delta\mathbf{L}_{WL}=\frac{f_1\nabla\Delta\mathbf{L}_1-f_2\nabla\Delta\mathbf{L}_2}{f_1-f_2}. \tag{4}$$

The rationale for this choice stems from the fact that, as far as ambiguity fixing is concerned, the longer wavelength of the GPS WL observations (86.2 cm), compared to GPS L1 (19.3 cm), has the effect of reducing the time to fix them [10]. Thus, we conjectured that a similar effect would arise in the case of computation of the generalized likelihood ratio.

Similarly, considering that for the GPS constellation and the L1 and L2C pair of frequencies, the standard deviation of the WL combination is about 5.74 times the standard deviation of each component (supposed to be equal), while the standard deviation of the Narrow Lane (NL) combination is about 0.71 times the standard deviation of each component, we resort here to the use of the NL combination $\nabla\Delta\mathbf{P}_{NL}$ [19], with

$$\nabla\Delta\mathbf{P}_{NL}=\frac{f_1\nabla\Delta\mathbf{P}_1+f_2\nabla\Delta\mathbf{P}_2}{f_1+f_2}. \tag{5}$$

From (2), (6), and (7), it follows that the measurement equations associated with $\nabla\Delta\mathbf{L}_{WL}$ and $\nabla\Delta\mathbf{P}_{NL}$ are

$$\begin{bmatrix}\nabla\Delta\mathbf{P}_{NL}\\ \nabla\Delta\mathbf{L}_{WL}\end{bmatrix}-\begin{bmatrix}\nabla\Delta\mathbf{r}(\hat{s}^0)\\ \nabla\Delta\mathbf{r}(\hat{s}^0)\end{bmatrix}-\begin{bmatrix}\nabla\Delta\hat{\boldsymbol{\beta}}^P_{NL}+c\nabla\Delta\hat{\mathbf{I}}_{NL}+c\nabla\Delta\hat{\mathbf{T}}\\ \nabla\Delta\hat{\boldsymbol{\beta}}^{\phi}_{WL}-c\nabla\Delta\hat{\mathbf{I}}_{WL}+c\nabla\Delta\hat{\mathbf{T}}\end{bmatrix}=$$
$$=\begin{bmatrix}\mathbf{HG}(\hat{s}^0) & \mathbf{0}\\ \mathbf{HG}(\hat{s}^0) & \lambda_{WL}\mathbf{I}\end{bmatrix}\begin{bmatrix}\Delta s\\ \nabla\Delta\mathbf{N}^{\phi}_{WL}\end{bmatrix}+\begin{bmatrix}\nabla\Delta\mathbf{n}^P_{NL}\\ \lambda_{WL}\nabla\Delta\mathbf{n}^{\phi}_{WL}\end{bmatrix}. \tag{6}$$

One advantage of the use of the pair ($\nabla\Delta\mathbf{L}_{WL}$, $\nabla\Delta\mathbf{P}_{NL}$) is that an initial estimate of the phase ambiguities range can be obtained by the Melbourne–Wübbena combination $\mathbf{B}_{MW}$, defined as follows [19]:

$$\mathbf{B}_{MW}=\mathbf{L}_{WL}-\mathbf{P}_{NL}. \tag{7}$$

In fact, as can be easily verified also from (6),

$$\nabla\Delta\mathbf{B}_{MW}=\nabla\Delta\mathbf{L}_{WL}-\nabla\Delta\mathbf{P}_{NL}=\lambda_{WL}\nabla\Delta\mathbf{N}^{\phi}_{WL}+$$
$$+\left(\nabla\Delta\hat{\boldsymbol{\beta}}^{\phi}_{WL}-\nabla\Delta\hat{\boldsymbol{\beta}}^{P}_{NL}\right)-c\left(\nabla\Delta\hat{\mathbf{I}}_{WL}+\nabla\Delta\hat{\mathbf{I}}_{NL}\right)+\mathbf{n}_{MW}, \tag{8}$$

where

$$\mathbf{n}_{MW}=\nabla\Delta\mathbf{n}^P_{NL}-\lambda_{WL}\nabla\Delta\mathbf{n}^{\phi}_{WL} \tag{9}$$

is the equivalent measurement noise on the Melbourne–Wübbena double differences.

As detailed in the next section, computation of the generalized likelihood ratio requires the evaluation of the estimate $\hat{s}_{\underset{\nabla\Delta\mathbf{N}_{WL}}{\sim\phi}}$ of the train mileage conditioned to a given phase ambiguity $\nabla\Delta\widetilde{\mathbf{N}}^{\phi}_{WL}$. Based on (6), $\hat{s}_{\underset{\nabla\Delta\mathbf{N}_{WL}}{\sim\phi}}$ is obtained by solving the linear system:

$$\begin{bmatrix}\mathbf{z}_P\\ \mathbf{z}_L\end{bmatrix}=\begin{bmatrix}\mathbf{I}\\ \mathbf{I}\end{bmatrix}\mathbf{HG}(\hat{s}^0)\Delta\hat{s}_{\nabla\Delta\widetilde{\mathbf{N}}^{\phi}_{WL}}+\begin{bmatrix}\nabla\Delta\mathbf{n}^P_{NL}\\ \lambda_{WL}\nabla\Delta\mathbf{n}^{\phi}_{WL}\end{bmatrix}, \tag{10}$$

where

$$\begin{bmatrix}\mathbf{z}_P\\ \mathbf{z}_L\end{bmatrix}\triangleq\begin{bmatrix}\nabla\Delta\mathbf{P}_{NL}\\ \nabla\Delta\mathbf{L}_{WL}\end{bmatrix}-\begin{bmatrix}\mathbf{0}\\ \lambda_{WL}\mathbf{I}\end{bmatrix}\nabla\Delta\widetilde{\mathbf{N}}^{\phi}_{WL}-\begin{bmatrix}\nabla\Delta\mathbf{r}(\hat{s}^0)\\ \nabla\Delta\mathbf{r}(\hat{s}^0)\end{bmatrix}$$
$$-\begin{bmatrix}\nabla\Delta\hat{\boldsymbol{\beta}}^P_{NL}+c\nabla\Delta\hat{\mathbf{I}}_{NL}+c\nabla\Delta\hat{\mathbf{T}}\\ \nabla\Delta\hat{\boldsymbol{\beta}}^{\phi}_{WL}-c\nabla\Delta\hat{\mathbf{I}}_{WL}+c\nabla\Delta\hat{\mathbf{T}}\end{bmatrix} \tag{11}$$

and then computing $\hat{s}_{\underset{\nabla\Delta\mathbf{N}_{WL}}{\sim\phi}}=\hat{s}^0+\Delta\hat{s}_{\underset{\nabla\Delta\mathbf{N}_{WL}}{\sim\phi}}$.

Let $\mathbf{R}_{P_{NL}}$ be the covariance matrix of $\nabla\Delta\mathbf{n}^P_{NL}$ and $\mathbf{R}_{L_{WL}}$ be the covariance matrix of $\lambda_{WL}\nabla\Delta\mathbf{n}^{\phi}_{WL}$. Then, when the weighted least square method is applied, the train mileage can be updated as follows:

$$\Delta\hat{s}_{\nabla\Delta\widetilde{\mathbf{N}}^{\phi}_{WL}}=\mathbf{K}\begin{bmatrix}\mathbf{z}_P\\ \mathbf{z}_L\end{bmatrix}, \tag{12}$$

where

$$\mathbf{K}=\left\{\mathbf{G}^T(\hat{s}^0)\mathbf{H}^T\left(\mathbf{R}^{-1}_{P_{NL}}+\mathbf{R}^{-1}_{L_{WL}}\right)\mathbf{HG}(\hat{s}^0)\right\}^{-1}$$
$$\mathbf{G}^T(\hat{s}^0)\mathbf{H}^T\left[\mathbf{R}^{-1}_{P_{NL}}\ \ \mathbf{R}^{-1}_{L_{WL}}\right]. \tag{13}$$

In addition, for the variance of the estimate, we obtain:

$$\sigma^2_{\Delta\hat{s}}=\left\{\mathbf{G}^T(\hat{s}^0)\mathbf{H}^T\left(\mathbf{R}^{-1}_{P_{NL}}+\mathbf{R}^{-1}_{L_{WL}}\right)\mathbf{HG}(\hat{s}^0)\right\}^{-1}. \tag{14}$$

Let us observe that when

$$\mathbf{R}_{P_{NL}}=\gamma_{PL}\mathbf{R}_{L_{WL}}, \tag{15}$$

the estimate $\Delta\hat{s}_{\underset{\nabla\Delta\mathbf{N}_{WL}}{\sim\phi}}$, given by (12), can be written as follows:

$$\Delta\hat{s}_{\nabla\Delta\widetilde{\mathbf{N}}^{\phi}_{WL}}=\frac{1}{1+\gamma_{PL}}\left(\Delta\hat{s}^P_{\underset{\nabla\Delta\mathbf{N}_{WL}}{\sim\phi}}+\gamma_{PL}\Delta\hat{s}^L_{\underset{\nabla\Delta\mathbf{N}_{WL}}{\sim\phi}}\right) \tag{16}$$

as the linear combination of the estimate $\Delta\hat{s}^P_{\underset{\nabla\Delta\mathbf{N}_{WL}}{\sim\phi}}$ based on $\nabla\Delta\mathbf{P}_{NL}$ only and of the estimate $\Delta\hat{s}^L_{\underset{\nabla\Delta\mathbf{N}_{WL}}{\sim\phi}}$ based only on $\nabla\Delta\mathbf{L}_{WL}$, respectively, given by

$$\Delta\hat{s}^P_{\underset{\nabla\Delta\mathbf{N}_{WL}}{\sim\phi}}=\mathbf{K}_{P_{NL}}\mathbf{z}_P, \tag{17}$$

$$\Delta\hat{s}^L_{\underset{\nabla\Delta\mathbf{N}_{WL}}{\sim\phi}}=\mathbf{K}_{L_{WL}}\mathbf{z}_L, \tag{18}$$

where

$$\mathbf{K}_{P_{NL}}=\left\{\mathbf{G}^T(\hat{s}^0)\mathbf{H}^T\mathbf{R}^{-1}_{P_{NL}}\mathbf{HG}(\hat{s}^0)\right\}^{-1}\mathbf{G}^T(\hat{s}^0)\mathbf{H}^T\mathbf{R}^{-1}_{P_{NL}}, \tag{19}$$

$$\mathbf{K}_{L_{WL}}=\left\{\mathbf{G}^T(\hat{s}^0)\mathbf{H}^T\mathbf{R}^{-1}_{L_{WL}}\mathbf{HG}(\hat{s}^0)\right\}^{-1}\mathbf{G}^T(\hat{s}^0)\mathbf{H}^T\mathbf{R}^{-1}_{L_{WL}}. \tag{20}$$

In fact, substituting (15) in (13), it follows that

$$\mathbf{K}=\left[\frac{1}{1+\gamma_{PL}}\mathbf{K}_{P_{NL}}\quad\frac{\gamma_{PL}}{1+\gamma_{PL}}\mathbf{K}_{L_{WL}}\right]. \tag{21}$$

Usually $\gamma_{PL}\gg 1$ and the contribution of the NL code component is negligible. Thus, to reduce the computational complexity, the train mileage estimate based on the WL carrier measurements only, after removing the ambiguities by means of the MW combination, can be adopted, as confirmed by the experimental results reported in section 6 (Experimental Results). Nevertheless, even in this case, the NL code pseudorange residuals still contribute to the track discrimination, as illustrated in the next section.

TRACK DETECTOR

For sake of compactness, in the following, we will denote with $\nabla\Delta\mathbf{R}$ the GNSS observables employed for the track discrimination and train location

determination, so that, when the pair $\nabla\Delta\mathbf{L}_{WL}$ and $\nabla\Delta\mathbf{P}_{NL}$ is employed, we have

$$\nabla\Delta\mathbf{R} = \begin{bmatrix} \nabla\Delta\mathbf{P}_{NL} \\ \nabla\Delta\mathbf{L}_{WL} \end{bmatrix}. \tag{22}$$

Then, assuming that there are M tracks on which the train may lie, denoting with H_k the hypothesis corresponding to the kth track, the generalized likelihood ratio $\Lambda_k(\nabla\Delta\mathbf{R})$ corresponding to H_k is given by the conditional probability density function of the observables $p_{\nabla\Delta\mathbf{R}/H_k}(\nabla\Delta\mathbf{R}/H_k)$ with respect to the kth hypothesis H_k divided by any arbitrary function that does not depend on H_k (see [16]):

$$\Lambda_k(\nabla\Delta\mathbf{R}) = \frac{p_{\nabla\Delta\mathbf{R}/H_k}(\nabla\Delta\mathbf{R}/H_k)}{w(\nabla\Delta\mathbf{R})}. \tag{23}$$

Assuming that the tracks are *a priori* identically distributed, the Bayesian (optimal) track detection rule selects the hypothesis corresponding to the largest $\Lambda_k(\nabla\Delta\mathbf{R})$.

However, considering that there is an additional set of unknowns given by the initial phase ambiguity double differences, we can rewrite Equation (23) as follows:

$$\Lambda_k(\nabla\Delta\mathbf{R}) = \\ = \frac{\sum\limits_{\nabla\Delta\widetilde{\mathbf{N}}^{\phi}_{WL}} p_{\nabla\Delta\mathbf{R}/H_k,\nabla\Delta\widetilde{\mathbf{N}}^{\phi}_{WL}}\left(\nabla\Delta\mathbf{R}/H_k,\nabla\Delta\widetilde{\widetilde{\mathbf{N}}}^{\phi}_{WL}\right)P\left(\nabla\Delta\widetilde{\widetilde{\mathbf{N}}}^{\phi}_{WL}/H_k\right)}{w(\nabla\Delta\mathbf{R})}. \tag{24}$$

On the other hand, we can assume the statistical independence between the initial phase ambiguities and the track on which the train is lying, so that we can write:

$$\Lambda_k(\nabla\Delta\mathbf{R}) = \\ = \frac{\sum\limits_{\nabla\Delta\widetilde{\mathbf{N}}^{\phi}_{WL}} p_{\nabla\Delta\mathbf{R}/H_k,\nabla\Delta\widetilde{\mathbf{N}}^{\phi}_{WL}}\left(\nabla\Delta\mathbf{R}/H_k,\nabla\Delta\widetilde{\widetilde{\mathbf{N}}}^{\phi}_{WL}\right)P\left(\nabla\Delta\widetilde{\widetilde{\mathbf{N}}}^{\phi}_{WL}\right)}{w(\nabla\Delta\mathbf{R})}. \tag{25}$$

Thus, proceeding as in [16], we first estimate the train mileage under the hypothesis that H_k and $\nabla\Delta\widetilde{\widetilde{\mathbf{N}}}^{\phi}_{WL}$ are true, and then, we use these estimates, let's say $\hat{s}_{H_k,\nabla\Delta\widetilde{\mathbf{N}}^{\phi}_{WL}}$ in a likelihood ratio test, as if they were correct. Thus, for each hypothesis and each set of phase ambiguity double differences, we compute the generalized likelihood functional $\widetilde{\Lambda}_k(\nabla\Delta\mathbf{R})$ as follows:

$$\widetilde{\Lambda}_k(\nabla\Delta\mathbf{R}) = \\ = \frac{\sum\limits_{\nabla\Delta\widetilde{\mathbf{N}}^{\phi}_{WL}} p_{\nabla\Delta\mathbf{R}/H_k,\nabla\Delta\widetilde{\mathbf{N}}^{\phi}_{WL}}\left(\nabla\Delta\mathbf{R}/\hat{s}_{H_k,\nabla\Delta\widetilde{\mathbf{N}}^{\phi}_{WL}},H_k,\nabla\Delta\widetilde{\widetilde{\mathbf{N}}}^{\phi}_{WL}\right)P\left(\nabla\Delta\widetilde{\widetilde{\mathbf{N}}}^{\phi}_{WL}/H_k\right)}{w(\nabla\Delta\mathbf{R})}. \tag{26}$$

Then, we select the hypothesis corresponding to the largest generalized likelihood functional.

Since conditioned to the kth hypothesis, and to the phase ambiguity $\nabla\Delta\widetilde{\widetilde{\mathbf{N}}}^{\phi}_{WL}$, $\nabla\Delta\mathbf{R}$ is a Gaussian random variable with (conditional) expectation

$$E\left\{\nabla\Delta\mathbf{R}/\hat{s}_{H_k,\nabla\Delta\widetilde{\mathbf{N}}^{\phi}_{WL}},H_k,\nabla\Delta\widetilde{\widetilde{\mathbf{N}}}^{\phi}_{WL}\right\} = \begin{bmatrix} \nabla\Delta\mathbf{r}\left(\hat{s}_{H_k,\nabla\Delta\widetilde{\mathbf{N}}^{\phi}_{WL}}\right) \\ \nabla\Delta\mathbf{r}\left(\hat{s}_{H_k,\nabla\Delta\widetilde{\mathbf{N}}^{\phi}_{WL}}\right) \end{bmatrix} \\ + \begin{bmatrix} \nabla\Delta\hat{\boldsymbol{\beta}}^{P}_{NL} + c\nabla\Delta\hat{\mathbf{I}}_{NL} + c\nabla\Delta\hat{\mathbf{T}} \\ \nabla\Delta\hat{\boldsymbol{\beta}}^{\phi}_{WL} - c\nabla\Delta\hat{\mathbf{I}}_{WL} + c\nabla\Delta\hat{\mathbf{T}} \end{bmatrix} + \begin{bmatrix} \mathbf{0} \\ \lambda_{WL}\mathbf{I} \end{bmatrix}\nabla\Delta\widetilde{\widetilde{\mathbf{N}}}^{\phi}_{WL}, \tag{27}$$

and covariance matrix

$$Cov\left\{\nabla\Delta\mathbf{R}/\hat{s}_{H_k,\nabla\Delta\widetilde{\mathbf{N}}^{\phi}_{WL}},H_k,\nabla\Delta\widetilde{\widetilde{\mathbf{N}}}^{\phi}_{WL}\right\} = \mathbf{R}_{\mathbf{v}_{WL}}, \tag{28}$$

we select

$$w(\nabla\Delta\mathbf{R}) = \frac{1}{\left[(2\pi)^{2(N_{sat}-1)}\det(\mathbf{R}_{v_{WL}})\right]}. \tag{29}$$

Then, denoting with $\mathbf{v}_{s_{H_k},\nabla\Delta\widetilde{\mathbf{N}}^{\phi}_{WL}}$ the vector

$$\mathbf{v}_{s_{H_k},\nabla\Delta\widetilde{\mathbf{N}}^{\phi}_{WL}} = \nabla\Delta\mathbf{R} - \begin{bmatrix} \nabla\Delta\mathbf{r}(s_{H_k}) \\ \nabla\Delta\mathbf{r}(s_{H_k}) \end{bmatrix} - \\ \begin{bmatrix} \nabla\Delta\hat{\boldsymbol{\beta}}^{P}_{NL} + c\nabla\Delta\hat{\mathbf{I}}_{NL} + c\nabla\Delta\hat{\mathbf{T}} \\ \nabla\Delta\hat{\boldsymbol{\beta}}^{\phi}_{WL} - c\nabla\Delta\hat{\mathbf{I}}_{WL} + c\nabla\Delta\hat{\mathbf{T}} \end{bmatrix} - \begin{bmatrix} \mathbf{0} \\ \lambda_{WL}\mathbf{I} \end{bmatrix}\nabla\Delta\widetilde{\widetilde{\mathbf{N}}}^{\phi}_{WL} \tag{30}$$

we have

$$\widetilde{\Lambda}_k(\nabla\Delta\mathbf{R}) = \\ = \underset{s_{H_k}}{\mathrm{Max}} \sum_{\nabla\Delta\widetilde{\widetilde{\mathbf{N}}}^{\phi}_{WL}} \exp\left\{-\frac{1}{2}\mathbf{v}^{T}_{s_{H_k},\nabla\Delta\widetilde{\mathbf{N}}^{\phi}_{WL}}\mathbf{R}^{-1}_{\mathbf{v}_{WL}}\mathbf{v}_{s_{H_k},\nabla\Delta\widetilde{\mathbf{N}}^{\phi}_{WL}}\right\}P\left(\nabla\Delta\widetilde{\widetilde{\mathbf{N}}}^{\phi}_{WL}\right). \tag{31}$$

Considering that in (24), each addendum is nonnegative, the estimate $\hat{s}_{H_k,\nabla\Delta\widetilde{\mathbf{N}}^{\phi}_{WL}}$ of s_{H_k} employed in track detection is the one for which each addendum is maximum, i.e.,

$$\hat{s}_{H_k,\nabla\Delta\widetilde{\mathbf{N}}^{\phi}_{WL}} = Arg\left\{\underset{s_{H_k}}{\mathrm{Min}}\left[\mathbf{v}^{T}_{s_{H_k},\nabla\Delta\widetilde{\mathbf{N}}^{\phi}_{WL}}\mathbf{R}^{-1}_{\mathbf{v}_{WL}}\mathbf{v}_{s_{H_k},\nabla\Delta\widetilde{\mathbf{N}}^{\phi}_{WL}}\right]\right\}. \tag{32}$$

Thus, for each potential phase ambiguity $\nabla\Delta\widetilde{\widetilde{\mathbf{N}}}^{\phi}_{WL}$, we first compute $\hat{s}_{H_k,\nabla\Delta\widetilde{\mathbf{N}}^{\phi}_{WL}}$ by means of Equation (12). Then, we compute the corresponding residual vector $\hat{\mathbf{v}}_{\hat{s}_{H_k,\nabla\Delta\mathbf{N}^{\phi}_{WL}},\nabla\Delta\widetilde{\widetilde{\mathbf{N}}}^{\phi}_{WL}}$ by means of Equation (30) by setting $s_{H_k} = \hat{s}_{H_k,\nabla\Delta\widetilde{\mathbf{N}}^{\phi}_{WL}}$.

The corresponding computational chain is illustrated in Figure 2. Here, $\nabla\Delta\mathbf{r}_{H_k}^{(h)}(\hat{s}^0)$ denotes the geometric range double difference referring to the point of the kth track with mileage $\hat{s}^0$. Differences between $\nabla\Delta\mathbf{r}_{H_k}^{(h)}(\hat{s}^0)$ and $\nabla\Delta\mathbf{r}_{H_h}^{(h)}(\hat{s}^0)$ are analyzed in Appendix B (see (B-6)).

Finally, we evaluate the generalized likelihood ratio $\widetilde{\Lambda}_k(\nabla\Delta\mathbf{R})$ as

$$\widetilde{\Lambda}_k(\nabla\Delta\mathbf{R}) = \sum_{\nabla\Delta\widetilde{\mathbf{N}}_{WL}^{\phi}\in\chi_\phi} \exp\left\{-\frac{1}{2}\left\|\hat{\mathbf{v}}_{\hat{s}_{H_k,\nabla\Delta\widetilde{\mathbf{N}}_{WL}^{\phi}},\nabla\Delta\widetilde{\mathbf{N}}_{WL}^{\phi}}\right\|^2_{\mathbf{R}_{\mathbf{v}_{WL}}^{-1}}\right\} P\left(\nabla\Delta\widetilde{\mathbf{N}}_{WL}^{\phi}\right), \tag{33}$$

where $\left\|\hat{\mathbf{v}}_{\hat{s}_{H_k,\nabla\Delta\mathbf{N}_{WL}^{\phi}},\nabla\Delta\mathbf{N}_{WL}^{\phi}}\right\|^2_{\mathbf{R}_{\mathbf{v}_{WL}}^{-1}}$ is the weighted squared L^2 norm of the residual with weight $\mathbf{R}_{\mathbf{v}_{WL}}^{-1}$:

$$\left\|\hat{\mathbf{v}}_{\hat{s}_{H_k,\nabla\Delta\mathbf{N}_{WL}^{\phi}},\nabla\Delta\mathbf{N}_{WL}^{\phi}}\right\|^2_{\mathbf{R}_{\mathbf{v}_{WL}}^{-1}} = \hat{\mathbf{v}}^T_{\hat{s}_{H_k,\nabla\Delta\mathbf{N}_{WL}^{\phi}},\nabla\Delta\mathbf{N}_{WL}^{\phi}}\mathbf{R}_{\mathbf{v}_{WL}}^{-1}\hat{\mathbf{v}}_{\hat{s}_{H_k,\nabla\Delta\mathbf{N}_{WL}^{\phi}},\nabla\Delta\mathbf{N}_{WL}^{\phi}}. \tag{34}$$

Then, the track detector will select the track with the largest $\widetilde{\Lambda}_k(\nabla\Delta\mathbf{R})$. Concerning the set χ_ϕ of Double Difference ambiguities employed in the computation of the generalized likelihood ratio (33), we restrict the computation to the set

$$\chi_\phi(\Delta_{MW}) = [\lfloor\nabla\Delta\mathbf{B}_{MW}\rfloor - \Delta_{MW}, \lceil\nabla\Delta\mathbf{B}_{MW}\rceil + \Delta_{MW}], \tag{35}$$

where $\lfloor x\rfloor$ is the greatest integer less than or equal to x, and $\lceil x\rceil$ is the least integer greater than or equal to x. The parameter δ_{MW} that controls the cardinality of Γ_ϕ is selected in accordance to the probability of including the true ambiguity in the computation, similarly to what was performed in the LAMBDA method to select the search set. In the experiments reported in section 6 (Experimental Results), considering that the receiver noise is low enough, δ_{MW} has been set to 1.

Let us observe that factoring $\mathbf{R}_{\mathbf{v}_{WL}}^{-1}$ as $\mathbf{R}_{\mathbf{v}_{WL}}^{-1} = \mathbf{C}_{\mathbf{v}_{WL}}^T\mathbf{C}_{\mathbf{v}_{WL}}$, we can rewrite the generalized likelihood ratio $\Lambda_k(\nabla\Delta\mathbf{R})$ in terms of a *normalized residual* vector with uncorrelated components with unit variance defined as follows:

$$\boldsymbol{\zeta}_{\hat{s}_{H_k,\nabla\Delta\widetilde{\mathbf{N}}_{WL}^{\phi}},\nabla\Delta\widetilde{\mathbf{N}}_{WL}^{\phi}} \cong \mathbf{C}_{\mathbf{v}_{WL}}\hat{\mathbf{v}}_{\hat{s}_{H_k,\nabla\Delta\widetilde{\mathbf{N}}_{WL}^{\phi}},\nabla\Delta\widetilde{\mathbf{N}}_{WL}^{\phi}}. \tag{36}$$

In fact from (34) and (36), we have

$$\left\|\hat{\mathbf{v}}_{\hat{s}_{H_k,\nabla\Delta\widetilde{\mathbf{N}}_{WL}^{\phi}},\nabla\Delta\widetilde{\mathbf{N}}_{WL}^{\phi}}\right\|^2_{\mathbf{R}_{\mathbf{v}_{WL}}^{-1}} = \left(\hat{\mathbf{v}}^T_{\hat{s}_{H_k,\nabla\Delta\widetilde{\mathbf{N}}_{WL}^{\phi}},\nabla\Delta\widetilde{\mathbf{N}}_{WL}^{\phi}}\mathbf{C}_{\mathbf{v}_{WL}}^T\right)\left(\mathbf{C}_{\mathbf{v}_{WL}}\hat{\mathbf{v}}_{\hat{s}_{H_k,\nabla\Delta\widetilde{\mathbf{N}}_{WL}^{\phi}},\nabla\Delta\widetilde{\mathbf{N}}_{WL}^{\phi}}\right) = \left\|\boldsymbol{\zeta}_{\hat{s}_{H_k,\nabla\Delta\widetilde{\mathbf{N}}_{WL}^{\phi}},\nabla\Delta\widetilde{\mathbf{N}}_{WL}^{\phi}}\right\|^2 \tag{37}$$

so that

$$\widetilde{\Lambda}_k(\nabla\Delta\mathbf{R}) = \sum_{\nabla\Delta\widetilde{\mathbf{N}}_{WL}^{\phi}\in\chi_\phi} \exp\left\{-\frac{1}{2}\left\|\boldsymbol{\zeta}_{\hat{s}_{H_k,\nabla\Delta\widetilde{\mathbf{N}}_{WL}^{\phi}},\nabla\Delta\widetilde{\mathbf{N}}_{WL}^{\phi}}\right\|^2\right\} P\left(\nabla\Delta\widetilde{\mathbf{N}}_{WL}^{\phi}\right). \tag{38}$$

In addition, the *a posteriori* probability of each hypothesis is approximated as follows:

$$\mathrm{Prob}\{H_k/\nabla\Delta\mathbf{R}\} = \frac{\sum_{\nabla\Delta\widetilde{\mathbf{N}}_{WL}^{\phi}\in\chi_\phi} \exp\left\{-\frac{1}{2}\left\|\boldsymbol{\zeta}_{\hat{s}_{H_k,\nabla\Delta\widetilde{\mathbf{N}}_{WL}^{\phi}},\nabla\Delta\widetilde{\mathbf{N}}_{WL}^{\phi}}\right\|^2\right\} P\left(\nabla\Delta\widetilde{\mathbf{N}}_{WL}^{\phi}\right)}{\sum_m \sum_{\nabla\Delta\widetilde{\mathbf{N}}_{WL}^{\phi}\in\chi_\phi} \exp\left\{-\frac{1}{2}\left\|\boldsymbol{\zeta}_{\hat{s}_{H_m,\nabla\Delta\widetilde{\mathbf{N}}_{WL}^{\phi}},\nabla\Delta\widetilde{\mathbf{N}}_{WL}^{\phi}}\right\|^2\right\} P\left(\nabla\Delta\widetilde{\mathbf{N}}_{WL}^{\phi}\right)}. \tag{39}$$

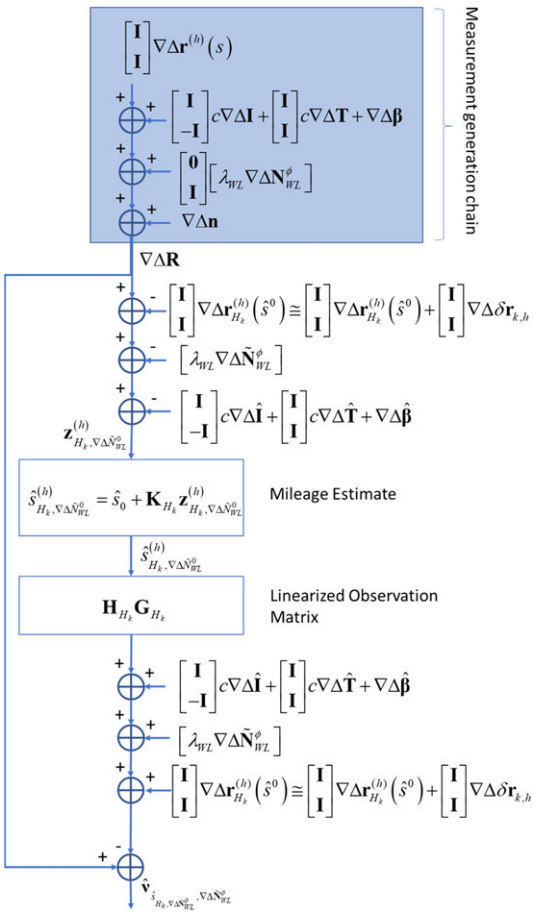

Fig. 2–Mileage and residual computational chain. [Color figure can be viewed at wileyonlinelibrary.com and www.ion.org]

TRACK DETECTOR PERFORMANCE

For the evaluation of the performance of the track detector, let us observe that, denoting with P_{e_h}, the probability of declaring that a train is on a wrong track conditioned to the event that the hth hypothesis is true and assuming *a priori* that the

M hypotheses are identically distributed, the error probability P_e of the track detector can be computed as follows:

$$P_e = \sum_{h=1}^{M} \frac{1}{M} P_{e_h}. \tag{40}$$

With reference to Figure 3, where the M tracks have been indexed from 1 to M, starting from left to right, we observe that for the computation of P_{e_h}, two different cases have to be accounted for either all the remaining tracks fall on the same side of the "true" track (corresponding to the hypotheses $h = 1$ and $h = M$) or the remaining tracks fall on both sides of the "true" track (corresponding to $1 < h < M$).

Thus, denoting with $P_{e_h}^{+}$ and $P_{e_h}^{-}$, the probability of deciding a wrong track respectively on the right side and on the left side of the true one, for the error probability, we have

$$P_e = P_{e_1}^{+} + \sum_{h=2}^{M-1} \frac{1}{M} \left(P_{e_h}^{-} + P_{e_h}^{+} \right) + P_{e_M}^{-}. \tag{41}$$

As detailed in Appendix B, $P_{e_h}^{+}$ and $P_{e_h}^{-}$ can be computed in a compact and meaningful way under the condition, met in practice, that the set of Double Difference ambiguities employed in the computation of the generalized likelihood ratio is the set $\chi_{\phi}(\delta_{MW})$ as defined in (35), with $\delta_{MW} \leq 2$. In fact under this condition, we may approximate the error probability as follows (see Equation (B-19)):

$$P_{e_h}^{\pm} \cong \frac{1}{2} erfc\left\{ \frac{\left\| \mathbf{\Gamma}_{h\pm1} \mathbf{d}_{h\pm1,\,h} \right\|}{2\sqrt{2}} \right\}, \tag{42}$$

where, as illustrated in Figure 3, $\mathbf{d}_{k,\,h}$ is the offset between the hth and the kth track, $\mathbf{\Gamma}_h$ is the matrix (see (B-9))

$$\mathbf{\Gamma}_k = -\mathbf{C}_{\mathbf{v}} (\mathbf{I} - \mathbf{H}_{H_h} \mathbf{G}_{H_h} \mathbf{K}_{H_h}) \begin{bmatrix} \mathbf{I} \\ \mathbf{I} \end{bmatrix} \mathbf{S}^{(j)} \mathbf{E}_{H_k} \tag{43}$$

and $erfc(\ )$ is the complementary error function, i.e.,

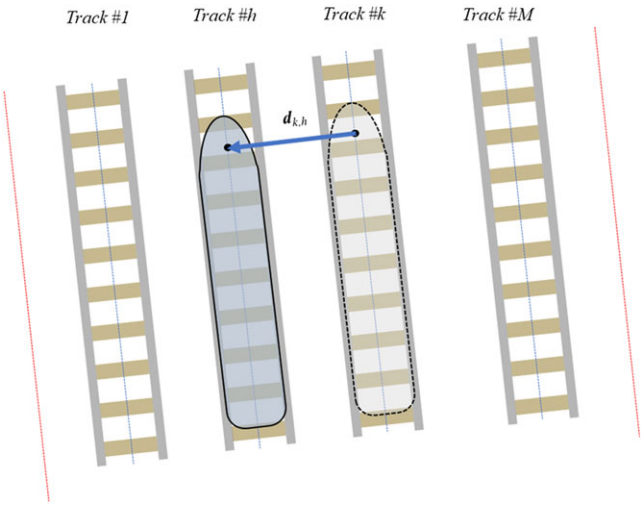

Fig. 3–Multiple tracks geometry. [Color figure can be viewed at wileyonlinelibrary.com and www.ion.org]

$$erfc(x) = \frac{2}{\sqrt{\pi}} \int_x^{\infty} e^{-t^2} dt. \tag{44}$$

In particular, for M parallel tracks with the same inter-axis distance Δd, we have:

$$P_e \cong \left(1 - \frac{1}{M} \right) erfc\left\{ \frac{\left\| \mathbf{\Gamma}_h \mathbf{e}_{\perp} \right\|}{2\sqrt{2}} \Delta d \right\}. \tag{45}$$

where $\mathbf{e}_{\perp}$ is the unit vector coplanar with the M tracks and orthogonal to the track tangent.

EXPERIMENTAL RESULTS

In order to test the developed algorithm for parallel track discrimination, raw data coming from the testbed installed in Sardinia (Italy) along the railway Cagliari – San Gavino (50 km) of RFI (Rete Ferroviaria Italiana) within the framework of the European Horizon 2020 ERSAT EAV project have been used (see Figure 4).

The testbed includes an augmentation network named TAAN (Track Area Augmentation Network), consisting of six Reference Stations deployed along the railway as illustrated in Figure 4, a Radio Block Center (RBC) deployed at the Cagliari Station facilities, and an Ale.668 train equipped with on-board equipment for train location determination, ERTMS train control, and connection of the train with the RBC.

The TAAN implements two layers of architecture (Local Networks + EGNOS Augmentation messages and relevant RIMS raw data) for Local Integrity Monitoring and computation of the Pseudorange corrections for the ERSAT EAV demonstration.

The Reference Stations have been installed on Public Administration buildings, following usual monumentation best practices, including Power Supply and remote TCP/IP connection. The Network is managed by the Sogei's GRNet Control Centre located in Rome (currently operating an institutional augmentation network in the center of Italy) for real-time monitoring, quality check, and hourly RINEX raw data collections. Specifications of the multi-constellation, multifrequency receivers are reported in Table 1.

The Location Determination System installed on board the train can employ several receivers. The tests reported here have been performed by means of a SEPTENTRIO ASTERX3 HDC receiver.

The results reported next refer to two different data sets. Data set #1 makes use of the pseudoranges collected by the Reference Stations located at the Villasor and Sanluri sites, with baseline of about 22 km. In particular, the data recorded at the Villasor site have been employed to feed the still

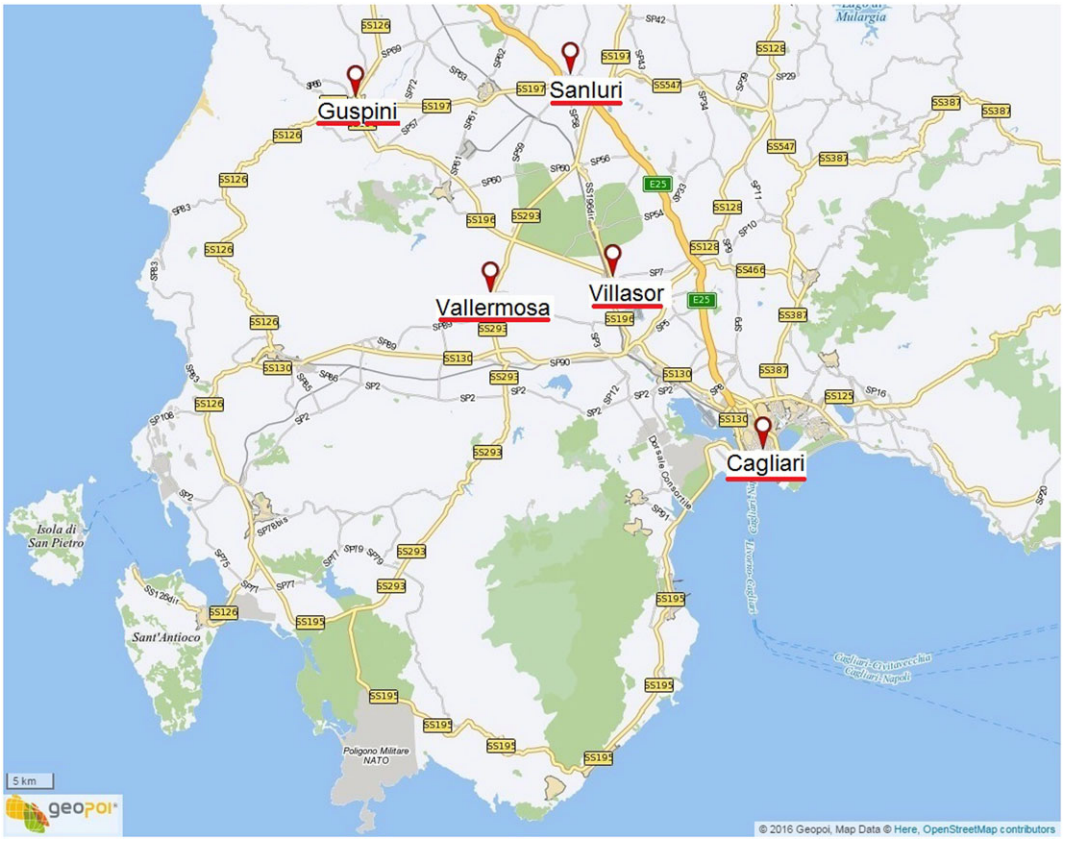

Fig. 4–ERSAT EAV Local Augmentation Network. [Color figure can be viewed at wileyonlinelibrary.com and www.ion.org]

train On-Board Unit emulator. To stress the performance validation, two parallel tracks with an inter-axis distance of 2.4 m have been simulated (compared to the larger value adopted in conventional lines), denoted in the following as Track #1 and Track #2. Track #1 is the track the train is on. Usage of this data set is motivated by the fact that the train location is completely known, and therefore, computation of the position error statistics is straight forward.

Data set #2 consists of data collected by the TAAN and by the SEPTENTRIO ASTERX3 HDC receiver installed on board the Ale.668 train during a run from San Gavino station to Cagliari station. The corresponding train mileage versus time is reported in Figure 5. In this scenario, two parallel tracks with an inter-axis distance of 3 m are present, with the train running on Track #1.

As illustrated by Figures 6 and 7, where a 1-h sample of the Melbourne–Wübbena combination

Table 1—Local Augmentation Reference Station characteristics

Tracking channels	120 channels GPS: L2, L2P, L2C, L5 GLONASS: L1 C/A, L2P, L2C Galileo: E1, E5a, E5b, E5a + b SBAS: WAAS, EGNOS, GAGAN, MSAS
Measurements quality	Very low noise GNSS carrier phase measurements (RMS < 0.2 mm)
Fixed ambiguities RTK positioning accuracy	10 mm + 1 ppm (horizontal) 10 mm + 1 ppm (vertical)
Antenna	Standard Dorne Margoline with choke ring antenna
Communication protocols/standards	NTRIP 2.0, RTCM 3.1
Measurements update rate	Up to 50 Hz

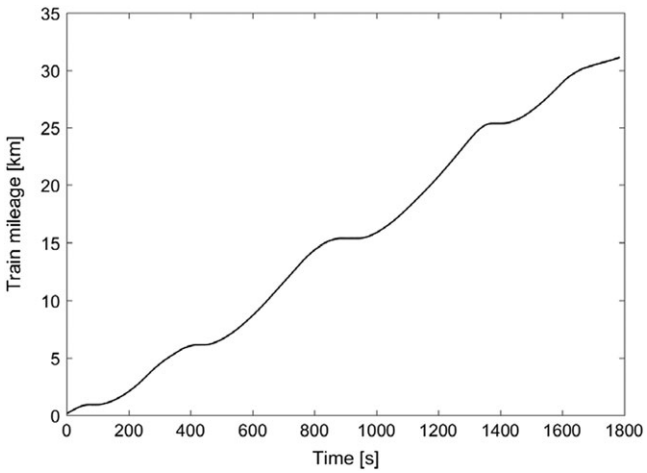

Fig. 5–Data set #2: Train mileage versus time.

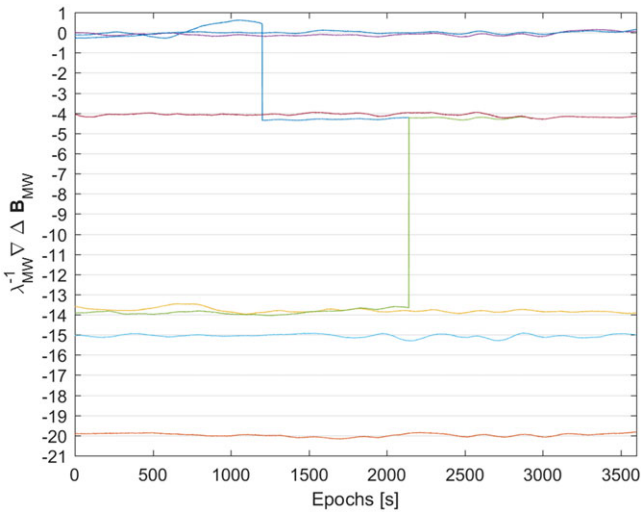

Fig. 6–Data set #2: Melbourne–Wübbena combination double difference of the recorded time series of two Reference Stations. [Color figure can be viewed at wileyonlinelibrary.com and www.ion.org]

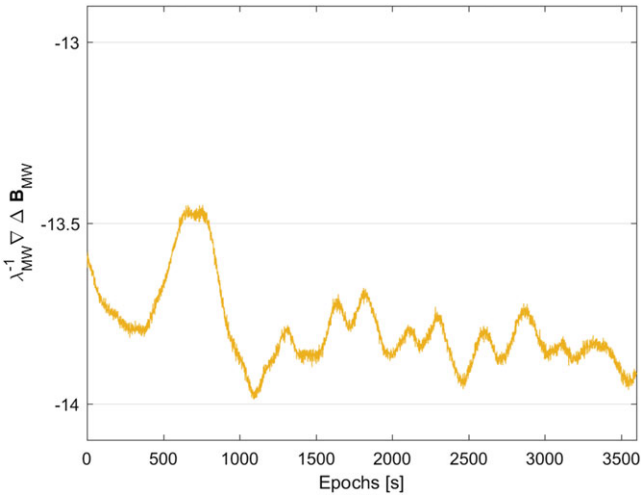

Fig. 7–Data set #2: Melbourne–Wübbena combination double difference of the recorded time series of two Reference Stations (detail of one double difference). [Color figure can be viewed at wileyonlinelibrary.com and www.ion.org]

double differences, scaled by the wide-lane wavelength ($\mathbf{B}_{MW}/\lambda_{WL}$) of data set #1, is reported, a very low frequency component due to multipath can affect the code channel. Nevertheless, noise amplitude is small enough so that only a few hypotheses may be considered for the receiver phase ambiguities. In practice, for each visible satellite whose elevation is large enough (e.g., >25°) to guarantee that the multipath effect is negligible, only two ambiguities corresponding to the ceiling and to the floor of the double difference of the Melbourne–Wübbena combination have been employed for track discrimination.

In Figures 8 and 9, the probabilities of the two tracks computed on an epoch by epoch basis, without any filtering of the receiver dynamics, for data sets

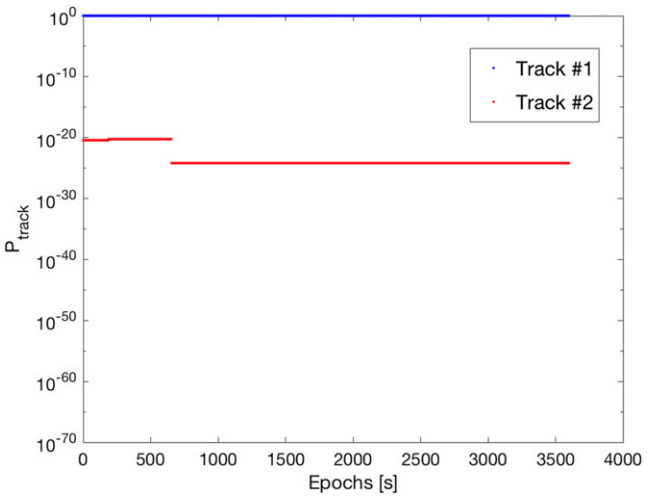

Fig. 8–Data set #1: Track a posteriori probability. [Color figure can be viewed at wileyonlinelibrary.com and www.ion.org]

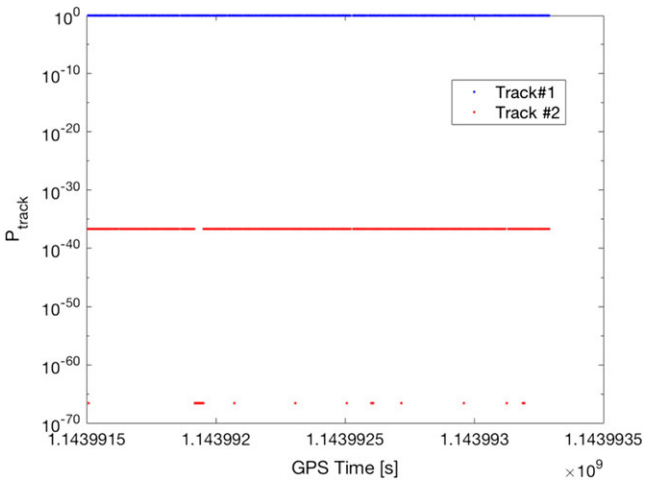

Fig. 9–Data set #2: Track a posteriori probability. [Color figure can be viewed at wileyonlinelibrary.com and www.ion.org]

#1 and #2 are reported. From these figures, it is evident that the probability of the true track (Track #1 for both data sets) largely exceeds that corresponding to the false hypothesis. Thus, no false discrimination has been observed in the elapsed time.

Concerning the accuracy of the train location, in Figure 10, the time series of the error of the train mileage estimation based on the maximum likelihood criterion for data set #1 is shown. The mean value of the error is −1.2 cm, while the standard deviation is 5 cm, and the mean square error is about 5.2 cm.

When only the narrow lane is employed, the mean value of the error is −0.7 cm, and the standard deviation is about 5.77 with a mean square error of about 5.8 cm.

In Figure 11, the corresponding Normal Probability plot is depicted. Let us recall that in the Normal Probability plot, the sample quantiles are plotted in such a way that the resulting pattern appears as a straight line when the data are samples

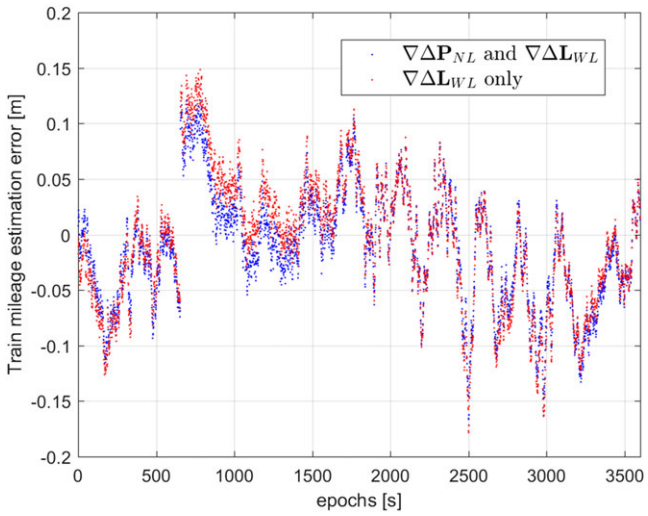

Fig. 10–Data set #1: Train mileage estimation error versus time. [Color figure can be viewed at wileyonlinelibrary.com and www.ion.org]

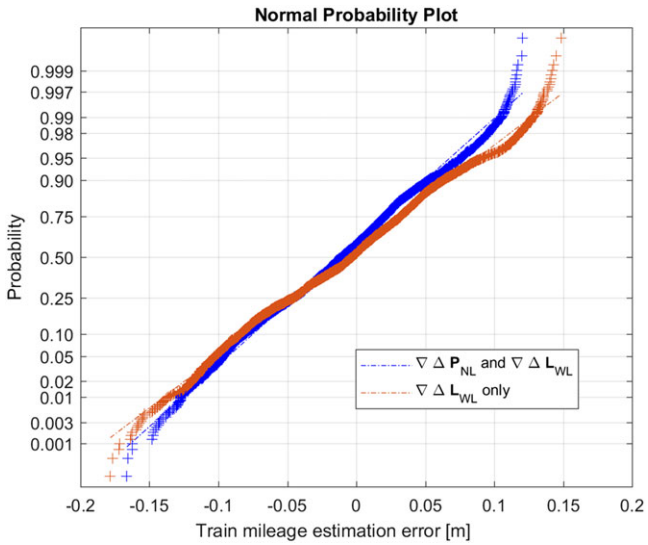

Fig. 11–Data set #1: Normal plot of the train mileage estimation error. [Color figure can be viewed at wileyonlinelibrary.com and www.ion.org]

from a Gaussian distribution. Since the estimation error is a nonstationary random time series, each sample has been normalized with respect to the standard deviation given by (14), before computing the Normal Probability plot.

The normal plot evidences that while the central part of the error distribution is well approximated by the normal distribution, it has heavier tail than the normal distribution.

Nevertheless, the largest magnitude of the error of the estimate obtained by jointly processing the Wide Lane carrier phase and Narrow Lane code combinations is about 20 cm and therefore is fairly well below the value required by ERTMS for the virtual balise localization. Thus, there is no need to solve the Narrow Lane carrier phase ambiguity.

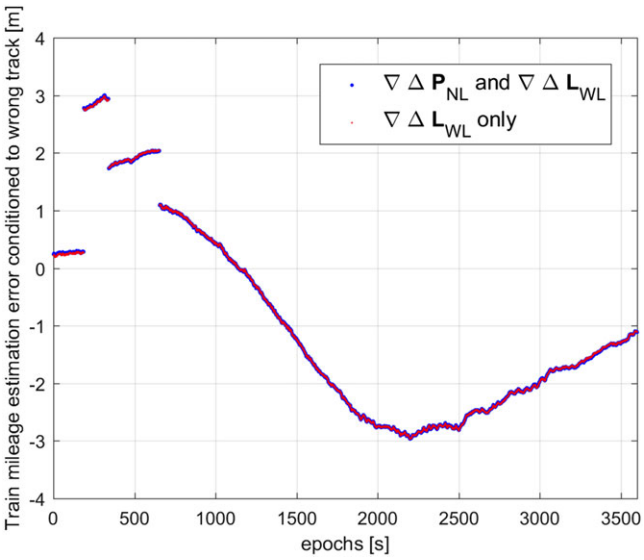

Fig. 12–Data set #1: Train mileage estimation error corresponding to Track #2 hypothesis. [Color figure can be viewed at wileyonlinelibrary.com and www.ion.org]

As illustrated by Figure 12, when computing the train mileage under the hypothesis that the train is lying on the other (wrong) track, the estimation error becomes quite large. The same behavior is exhibited by the pseudorange residuals.

We finally observe that joint use of phase and code combinations, although reducing the average accuracy due to the use of the code derived information, which is in fact noisier than the carrier phase information, prevents degradations due to phase ambiguity mismatching.

CONCLUSIONS

In this paper, we presented a novel solution for discrimination of a train's track at the Start of Mission, based on a high precision algorithm that makes use of the Wide Lane carrier phase and Narrow Lane code combinations, together with the track constraint to evaluate the posterior probability of each track.

As confirmed by the experimental activity, the coarse estimate of the train location provided by the Wide Lane combination is good enough to reliably determine the track. The main advantage is the trade-off between accuracy and time needed to accomplish this. In fact, in our case, we do not have to wait for ambiguity fixing.

To achieve track error probabilities compatible with SIL-4 operational requirements even in strong multipath environments, temporal integration and multiple constellations can be applied. Nevertheless, effectiveness of temporal integration can be impaired by multipath errors highly correlated in time. To reduce this effect, proceeding at the

maximum speed allowed when in Start of Mission mode, as in the current procedure, is recommended.

APPENDIX A. TRACK CONSTRAINED RELATIVE PVT ESTIMATE

Let $\phi_{i,p}^{Train}(k)$ and $\phi_{i,p}^{MS}(k)$ be the carrier phases of the signal with carrier frequency f_i (and wavelength λ_i), transmitted by the pth satellite at kth epoch and respectively received by the OBU GNSS receiver and by the Master Station (MS). They can be expressed as

$$\phi_{i,p}^{Train}(k) = \frac{1}{\lambda_i}\Big[r_{Train}^{p}(k) + N_{i,p}^{Train}\lambda_i - cI_{i_{Train}}^{p}(k) + cT_{Train}^{p}(k) + \\ +c\delta t^{Train}(k) - c\delta t_{i,p}^{Sat}(k) + \beta_{i,p}^{\phi,Train}(k) + n_{i,p}^{\phi,Train}(k)\Big] \tag{A-1}$$

$$\phi_{i}^{MS}(k) = \frac{1}{\lambda_i}\Big[r_{MS}^{p}(k) + N_{i,p}^{MS}\lambda - cI_{i_{MS}}^{p}(k) + cT_{MS}^{p}(k) + \\ +c\delta t^{MS}(k) - c\delta t_{i,p}^{Sat}(k) + \beta_{i,p}^{\phi,MS}(k) \\ +n_{i}^{\phi,MS}(k)\Big], \tag{A-2}$$

where

- $r_{Train}^{p}(k) = \left\|\mathbf{X}_{p}^{Sat}[k] - \mathbf{X}^{Train}[s(k)]\right\|$ is the geometric distance between the pth satellite located in $\mathbf{X}_{p}^{Sat}[k]$ and the receiver on board of the train located in $\mathbf{X}^{Train}[s]$;
- $r_{MS}^{p}(k) = \left\|\mathbf{X}_{p}^{Sat}[k] - \mathbf{X}^{MS}\right\|$ is the geometric distance between the pth satellite located in $\mathbf{X}_{p}^{Sat}[k]$ and the MS receiver located in $\mathbf{X}^{MS}$;
- N_i^{MS} and N_i^{Train} are the carrier phase offsets (in multiples of the wavelength) of the MS and Train receivers;
- $I_{i_{MS}}^{p}(k)$, $I_{i_{Train}}^{p}(k)$, $T_{MS}^{p}(k)$, and $T_{Train}^{p}(k)$ are the ionospheric and tropospheric delays along the paths from the pth satellite to the GNSS receivers (i.e., respectively, the *MS* and the OBU GNSS receiver) for the kth epoch;
- $\delta t_{i,p}^{Sat}(k)$ is the offset of the pth satellite clock for the kth epoch;
- $\delta t^{Train}(k)$ and $\delta t^{MS}(k)$ are the train's and *MS*'s receiver clock offsets;
- $n_{i,p}^{\phi,MS}(k)$ and $n_{i,p}^{\phi,Train}(k)$ are the errors of the time of arrival estimation algorithm, generated by multipath, GNSS receiver thermal noise, and eventual radio frequency interference, respectively, at the *MS* and the OBU GNSS receiver; and,
- $\beta_{i,p}^{MS}(k)$ and $\beta_{i,p}^{Train}(k)$ are the biases, accounting for differences in latency and delay among channels, at both sides, satellite and receiver, as well as the wind-up effect and antenna phase centers.

For sake of compactness in the following, we omit the epoch index k. Let $\mathbf{b}(s)$ be the baseline between the reference station located in $\mathbf{X}^{MS}$ and the GNSS receiver located in $\mathbf{X}^{Train}(s)$ corresponding to mileage s, i.e.,

$$\mathbf{b}(s) = \mathbf{X}^{Train}(s) - \mathbf{X}^{MS}, \tag{A-3}$$

and let $\mathbf{e}_{Train}^{p}(s)$ and $\mathbf{e}_{MS}^{p}$ be the unit vectors corresponding to the lines-of-sight from the pth satellite to the OBU and to the *MS* GNSS receiver, respectively:

$$\mathbf{e}_{Train}^{p}(s) = \frac{\mathbf{X}_{p}^{Sat} - \mathbf{X}^{Train}(s)}{\left\|\mathbf{X}_{p}^{Sat} - \mathbf{X}^{Train}(s)\right\|}, \quad \mathbf{e}_{MS}^{p} = \frac{\mathbf{X}_{p}^{Sat} - \mathbf{X}^{MS}}{\left\|\mathbf{X}_{p}^{Sat} - \mathbf{X}^{MS}\right\|}. \tag{A-4}$$

Then, for the single difference between the geometric distances between the pth satellite and the *MS* and the OBU GNSS receiver, we can write:

$$r_{Train}^{p}(s) - r_{MS}^{p} = \left[1 - \left(\mathbf{e}_{MS}^{p}\right)^{T}\mathbf{e}_{Train}^{p}(s)\right]r_{Train}^{p}(s) \\ -\left(\mathbf{e}_{MS}^{p}\right)^{T}\mathbf{b}(s). \tag{A-5}$$

Then, denoting with $\mathbf{e}_{MS}$ and $\mathbf{e}_{Train}(s)$, the arrays of the line of sight unit vectors

$$\mathbf{e}_{MS} = \left[\mathbf{e}_{MS}^{1} \quad \mathbf{e}_{MS}^{2} \quad \dots \quad \mathbf{e}_{MS}^{N_{sat}}\right], \tag{A-6}$$

$$\mathbf{e}_{Train}(s) = \left[\mathbf{e}_{Train}^{1}(s) \quad \mathbf{e}_{Train}^{2}(s) \quad \dots \quad \mathbf{e}_{Train}^{N_{sat}}(s)\right], \tag{A-7}$$

Equation (A-5) can be written in matrix form as follows:

$$\mathbf{r}_{Train}(s) - \mathbf{r}_{MS} = \left(\mathbf{I} - \mathbf{I}\circ\mathbf{e}_{Train}^{T}(s)\mathbf{e}_{MS}\right)\mathbf{r}_{Train}(s) \\ -\mathbf{e}_{MS}^{T}\mathbf{b}(s), \tag{A-8}$$

where $\circ$ is the Hadamard matrix product (so that given two matrices $\mathbf{B}$ and $\mathbf{C}$, $(\mathbf{B}\circ\mathbf{C})_{ij} = B_{ij}C_{ij}$).

Let us assume, without loss of generality, that the jth satellite is used as pivot (see Figure 13). Then, denoting with $\mathbf{S}^{(j)}$ the partitioned matrix

$$\mathbf{S}^{(j)} = \begin{bmatrix} -\mathbf{I}_{j-1} & \mathbf{1}_{j-1} & 0 \\ 0 & \mathbf{1}_{N_{Sat}-j} & -\mathbf{I}_{N_{Sat}-j} \end{bmatrix}, \tag{A-9}$$

where $\mathbf{I}_M$ denotes the identity matrix of size M and $\mathbf{1}_M$ is a column vector of size $M \times 1$ with elements equal to 1, the single difference of a satellite observable $\boldsymbol{\zeta}$ can be written as

$$\Delta\boldsymbol{\zeta} = \mathbf{S}^{(j)}\boldsymbol{\zeta}, \tag{A-10}$$

while for the double difference, we have

$$\nabla\Delta\boldsymbol{\zeta} = \left[\mathbf{S}^{(j)} \quad -\mathbf{S}^{(j)}\right]\begin{bmatrix}\boldsymbol{\zeta}^{Train} \\ \boldsymbol{\zeta}^{MS}\end{bmatrix}. \tag{A-11}$$

Therefore, the column array $\nabla\Delta\mathbf{L}_i = \lambda_i\nabla\Delta\boldsymbol{\phi}_i$ of the double differences of the carrier phase pseudoranges (expressed in meters) at frequency f_i with elements

$$\left[\nabla\Delta\mathbf{L}_i\right]_{p,1} = \lambda_i\left\{\phi_j^{Train}(k) - \phi_j^{MS}(k) - \left[\phi_p^{Train}(k) - \phi_p^{MS}(k)\right]\right\} \tag{A-12}$$

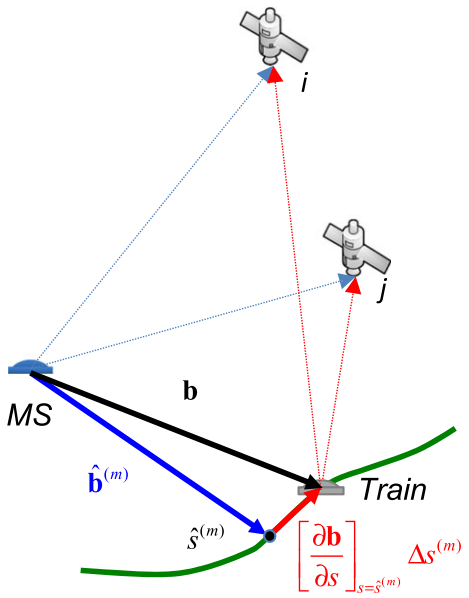

Fig. 13–Baseline geometry. [Color figure can be viewed at wileyonlinelibrary.com and www.ion.org]

can be written as follows:

$$\nabla\Delta\mathbf{L}_i = \lambda_i \begin{bmatrix} \mathbf{S}^{(j)} & -\mathbf{S}^{(j)} \end{bmatrix} \begin{bmatrix} \boldsymbol{\phi}_i^{Train} \\ \boldsymbol{\phi}_i^{MS} \end{bmatrix}. \tag{A-13}$$

On the other hand, from (A-8), it follows that the double difference of the geometric distance $\nabla\Delta\mathbf{r}(s)$ is given by

$$\begin{aligned} \nabla\Delta\mathbf{r}(s) &= \begin{bmatrix} \mathbf{S}^{(j)} & -\mathbf{S}^{(j)} \end{bmatrix} \begin{bmatrix} \mathbf{r}_{Train}(s) \\ \mathbf{r}_{MS} \end{bmatrix} = \\ &= \mathbf{S}^{(j)} \left(\mathbf{I} - \mathbf{I} \circ \mathbf{e}_{Train}^T(s)\mathbf{e}_{MS}\right)\mathbf{r}_{Train}(s) - \mathbf{S}^{(j)}\mathbf{e}_{MS}^T\mathbf{b}(s), \end{aligned} \tag{A-14}$$

so that the double-difference measurement equation can be rewritten in matrix form as follows:

$$\begin{aligned} &\nabla\Delta\mathbf{L}_i - \Delta\mathbf{DD}(s) + c\nabla\Delta\mathbf{I}_i - c\nabla\Delta\mathbf{T} - \nabla\Delta\boldsymbol{\beta}_i^{\phi} = \\ &= \lambda\nabla\Delta\mathbf{N}_i^{\phi} + \mathbf{H}\mathbf{b}(s) + \nabla\Delta\mathbf{n}_i^{\phi}, \end{aligned} \tag{A-15}$$

where

$$\Delta\mathbf{DD}(s) = \mathbf{S}^{(j)}\left(\mathbf{I} - \mathbf{I} \circ \mathbf{e}_{Train}^T(s)\mathbf{e}_{MS}\right)\mathbf{r}_{Train}(s) \tag{A-16}$$

is the term accounting for the differences between the satellite line of sights of the MS and the OBU receiver, and $\mathbf{H}$ is the matrix of differences of the

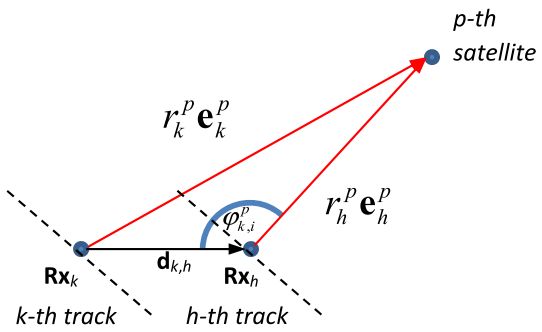

Fig. 14–Parallel track geometry. [Color figure can be viewed at wileyonlinelibrary.com and www.ion.org]

directional cosines of the line of sight unit vectors with respect to the pivot:

$$\mathbf{H} = \mathbf{S}^{(i)}\mathbf{e}_{MS}^T. \tag{A-17}$$

Incidentally, we observe that (A-11) implies that we can express the covariance matrix of $\nabla\Delta\mathbf{n}_i^{\phi}$ in terms of the covariance matrices

$$\mathbf{R}_{n_{Train}} = \mathrm{diag}\left(\sigma^2_{n_{Train_1}}, \sigma^2_{n_{Train_2}}, \ldots, \sigma^2_{n_{Train_{N_{sat}}}}\right), \tag{A-18}$$

$$\mathbf{R}_{n_{MS}} = \mathrm{diag}\left(\sigma^2_{n_{MS_1}}, \sigma^2_{n_{MS_2}}, \ldots, \sigma^2_{n_{MS_{N_{sat}}}}\right), \tag{A-19}$$

of the equivalent receiver noise, as follows:

$$\mathbf{R}_{\Delta\nabla\mathbf{n}_i^{\phi}} = \begin{bmatrix} \mathbf{S}^{(j)} & -\mathbf{S}^{(j)} \end{bmatrix} \begin{bmatrix} \mathbf{R}_{\mathbf{n}_i^{\phi,Train}} & 0 \\ 0 & \mathbf{R}_{\mathbf{n}_i^{\phi,MS}} \end{bmatrix} \begin{bmatrix} \mathbf{S}^{(j)} & -\mathbf{S}^{(j)} \end{bmatrix}^T. \tag{A-20}$$

To linearize the double-difference measurement Equation (A-15) with respect to the train mileage s, we observe that the sensitivity of $\Delta\mathbf{DD}(s)$ with respect to s is completely negligible when compared to $\mathbf{Hb}(s)$. Therefore, let $\hat{s}^0$ be an initial guess of the train mileage and $\mathbf{b}(\hat{s}^0)$ be the corresponding baseline:

$$\mathbf{b}(\hat{s}^0) = \mathbf{X}^{Train}[\hat{s}^0] - \mathbf{X}^{MS}. \tag{A-21}$$

Then, expanding the baseline in Taylor series with respect to s, with initial point $\hat{s}^0$, we have

$$\mathbf{b}(s) \cong \mathbf{b}(\hat{s}^0) + \left[\frac{\partial \mathbf{b}}{\partial s}\right]_{s=\hat{s}^0} \Delta s, \tag{A-22}$$

where $\Delta s = s - \hat{s}^0$. On the other hand,

$$\frac{\partial \mathbf{b}}{\partial s} = \frac{\partial \mathbf{X}^{Train}(s)}{\partial s} - \frac{\partial \mathbf{X}^{MS}}{\partial s} = \frac{\partial \mathbf{X}^{Train}(s)}{\partial s}, \tag{A-23}$$

therefore, denoting by $\mathbf{G}(\hat{s}^0)$ the vector of the tangent to track at the mileage $\hat{s}^0$:

$$\mathbf{G}(\hat{s}^0) = \left[\frac{\partial \mathbf{X}^{Train}}{\partial s}\right]_{s=\hat{s}^0}, \tag{A-24}$$

and substituting (A-24) and (A-22) in (A-15), the following linearized double-difference measurement equation is obtained:

$$\begin{aligned} &\nabla\Delta\mathbf{L}_i - \nabla\Delta\mathbf{r}(\hat{s}^0) - \nabla\Delta\boldsymbol{\beta}_i^{\phi} + c\nabla\Delta\mathbf{I}_i - c\nabla\Delta\mathbf{T} = \\ &= \lambda\nabla\Delta\mathbf{N}_i^{\phi} + \mathbf{H}\mathbf{G}(\hat{s}^0)\Delta s + \nabla\Delta\mathbf{n}_i^{\phi}, \quad i = 1, 2. \end{aligned} \tag{A-25}$$

Proceeding in the same way, for the double difference $\nabla\Delta\mathbf{P}_i$ of the code pseudoranges, we have

$$\begin{aligned} &\nabla\Delta\mathbf{P}_i - \nabla\Delta\mathbf{r}(\hat{s}^0) - \nabla\Delta\boldsymbol{\beta}_i^{P} - c\nabla\Delta\mathbf{I}_i - c\nabla\Delta\mathbf{T} = \\ &= \mathbf{H}\mathbf{G}(\hat{s}^0)\Delta s + \nabla\Delta\mathbf{n}_i^{P}, \quad i = 1, 2. \end{aligned} \tag{A-26}$$

We note the opposite sign of the ionospheric incremental time delay in the code and carrier phase equations.

Concerning the double differences of the ionospheric and tropospheric delays, for large baselines, or in the presence of strong spatial gradients of those delays, a joint estimation of them can be performed remembering that the ionospheric incremental delay can be expressed in terms of Slant TEC (STEC), so that

$$c\nabla\Delta\mathbf{I}_i \cong \frac{40.3\cdot 10^{16}}{f_i^2}\nabla\Delta\mathbf{STEC}. \tag{A-27}$$

Rearranging Equations (A-25) and (A-26) into a single linear system, Equation (2) follows. For sake of simplicity, in the derivation of Equation (2), we considered the case in which the estimates $\nabla\Delta\hat{\mathbf{I}}_i$ and $\nabla\Delta\hat{\mathbf{T}}$ of the double differences of the ionospheric and tropospheric delays obtained from the best available models are available. Otherwise, $\nabla\Delta\hat{\mathbf{I}}_i$ and $\nabla\Delta\hat{\mathbf{T}}$ are inserted in the unknowns, as in the ordinary RTK method.

APPENDIX B. TRACK DETECTION ERROR PROBABILITY

For the computation of $P_{e_h}^{\pm}$, we observe that the detector will perform a wrong decision whenever there is at least one track, say the kth one, on the proper side of the true one, for which the generalized likelihood ratio $\widetilde{\Lambda}_k^{(h)}$ conditioned to the event that the train is operating on the hth track, i.e.,

$$\widetilde{\Lambda}_k^{(h)} = \sum_{\nabla\Delta\widetilde{\mathbf{N}}_{WL}^{\phi}\in\chi_\phi} \exp\left\{-\frac{1}{2}\left\|\boldsymbol{\zeta}^{(h)}_{\hat{s}_{H_k,\nabla\Delta\widetilde{\mathbf{N}}_{WL}^{\phi}},\nabla\Delta\widetilde{\mathbf{N}}_{WL}^{\phi}}\right\|^2\right\} P\left(\nabla\Delta\widetilde{\mathbf{N}}_{WL}^{\phi}\right) \tag{B-1}$$

is greater than $\widetilde{\Lambda}_h^{(h)}$, where in (B-1), we denoted with $\boldsymbol{\zeta}^{(h)}_{\hat{s}_{H_k,\nabla\Delta\widetilde{\mathbf{N}}_{WL}^{\phi}},\nabla\Delta\widetilde{\mathbf{N}}_{WL}^{\phi}}$ the normalized residual corresponding to the kth hypothesis, under the condition that the train is operating on the hth track.

To evaluate the probability that $\widetilde{\Lambda}_k^{(h)} > \widetilde{\Lambda}_h^{(h)}$, let us first express the normalized residual $\boldsymbol{\zeta}^{(h)}_{\hat{s}_{H_k,\nabla\Delta\widetilde{\mathbf{N}}_{WL}^{\phi}},\nabla\Delta\widetilde{\mathbf{N}}_{WL}^{\phi}}$ in terms of $\boldsymbol{\zeta}^{(h)}_{\hat{s}_{H_h,\nabla\Delta\mathbf{N}_{WL}^{\phi}},\nabla\Delta\mathbf{N}_{WL}^{\phi}}$.

To this end, with reference to Figure 14, let us denote with s the current train mileage and with $\mathbf{Rx}_h$ the corresponding point of the hth track. In addition, let $\mathbf{d}_{k,h}$ be the offset between the hth and the kth track and $\mathbf{Rx}_k$ the point of the kth track obtained by applying the offset $\mathbf{d}_{k,h}$ to $\mathbf{Rx}_h$. For sake of compactness, without loss of generality, let us assume that the two tracks always run in parallel so that the mileage of $\mathbf{Rx}_h$ and $\mathbf{Rx}_k$ is the same.

Then we can estimate the train mileage for the kth track by using $\mathbf{Rx}_k$ as the initial point of the linearization procedure. At this point, in order to apply Equations (11) and (12), we first have to compute the geometric distance double difference $\nabla\Delta\mathbf{r}_{H_k}^{(h)}$ corresponding to $\mathbf{Rx}_k$.

We observe that the geometric distance r_k^p between the pth satellite and $\mathbf{Rx}_k$ can be written in terms of the geometric distance r_h^p between the pth satellite and the point $\mathbf{Rx}_h$ as follows:

$$r_k^p\mathbf{e}_k^p = \mathbf{d}_{k,h} + r_h^p\mathbf{e}_h^p, \mathbf{e}_k^p\mathbf{e}_k^p = \mathbf{d}_{k,h}, \mathbf{e}_k^p\mathbf{e}_k^p + r_h^p\mathbf{e}_h^p, \mathbf{e}_k^p\mathbf{e}_k^p, \tag{B-2}$$

where $\mathbf{e}_k^p$ and $\mathbf{e}_h^p$ are the satellite line of sight unit vectors with respect to $\mathbf{Rx}_k$ and $\mathbf{Rx}_h$ and $<\ ,>$ is the scalar product operator.

Thus, the difference between the two geometric distances is

$$\begin{aligned}\delta r_{k,h}^p &= r_k^p - r_h^p = \\ &= r_h^p\left[\left\langle\mathbf{e}_h^p, \mathbf{e}_k^p\right\rangle - 1\right] + \left\langle\mathbf{d}_{k,h}, \mathbf{e}_k^p\right\rangle.\end{aligned} \tag{B-3}$$

In practice, since the offsets are rather small, we have

$$\delta r_{k,h}^p \cong \left\langle\mathbf{d}_{k,h}, \mathbf{e}_k^p\right\rangle. \tag{B-4}$$

The above relation can be written in matrix form as follows:

$$\delta\mathbf{r}_{k,h} = \mathbf{E}_{H_k}\mathbf{d}_{k,h}, \tag{B-5}$$

where $\mathbf{E}_{H_k}$ is the directional cosine matrix associated with the satellite lines-of-sight with respect to the receiver lying on the hth track. Thus, the geometric distance double differences corresponding to the kth hypothesis when the hth one is true present an additional term given by

$$\nabla\Delta\delta\mathbf{r}_{k,h} = \mathbf{S}^{(j)}\mathbf{E}_{H_k}\mathbf{d}_{k,h}, \tag{B-6}$$

where $\mathbf{S}^{(j)}$ is the partitioned matrix given by (A-9), that computes the single difference with respect to the jth satellite. Incidentally, we observe that, due to the fact that the offset between the tracks is just a few meters, $\mathbf{E}_{H_k}$ and $\mathbf{E}_{H_h}$ are practically equal.

Thus, denoting with $\hat{s}_{H_k,\nabla\Delta\widetilde{\mathbf{N}}_{WL}^{\phi}/H_h}$ the estimate of the train mileage on the kth track corresponding to the phase ambiguity $\nabla\Delta\widetilde{\mathbf{N}}_{WL}^{\phi}$ when the true track is the hth one, as illustrated in Figure 2 where the residual computation chain is reported, we have

$$\hat{s}_{H_k,\nabla\Delta\widetilde{\mathbf{N}}_{WL}^{\phi}/H_h} = \hat{s}_{H_h,\nabla\Delta\widetilde{\mathbf{N}}_{WL}^{\phi}} - \mathbf{K}_{H_k}\begin{bmatrix}\nabla\Delta\delta\mathbf{r}_{k,h}\\ \nabla\Delta\delta\mathbf{r}_{k,h}\end{bmatrix}. \tag{B-7}$$

Therefore,

$$\boldsymbol{\zeta}^{(h)}_{\hat{s}_{H_k,\nabla\Delta\widetilde{\mathbf{N}}_{WL}^{\phi}},\nabla\Delta\widetilde{\mathbf{N}}_{WL}^{\phi}} = \boldsymbol{\zeta}^{(h)}_{\hat{s}_{H_h,\nabla\Delta\widetilde{\mathbf{N}}_{WL}^{\phi}},\nabla\Delta\widetilde{\mathbf{N}}_{WL}^{\phi}} + \boldsymbol{\Gamma}_k\mathbf{d}_{k,h}, \tag{B-8}$$

where

$$\boldsymbol{\Gamma}_k = -\mathbf{C}_{\mathbf{v}}(\mathbf{I} - \mathbf{H}_{H_h}\mathbf{G}_{H_h}\mathbf{K}_{H_h})\begin{bmatrix}\mathbf{I}\\ \mathbf{I}\end{bmatrix}\mathbf{S}^{(j)}\mathbf{E}_{H_k}. \tag{B-9}$$

In addition, let $\nabla\Delta\mathbf{N}_{WL}^{\phi}$ be the true phase ambiguity double difference. Then, based on (11), we have that

the estimate $\hat{s}_{H_h,\nabla\Delta\tilde{\mathbf{N}}^{\phi}_{WL}/H_h}$ of the mileage of the train, under the hypothesis that the train is operating on the hth track corresponding to the phase ambiguity $\nabla\Delta\tilde{\mathbf{N}}^{\phi}_{WL}$, is related to the estimate $\hat{s}_{H_h,\nabla\Delta N^{\phi}_{WL}/H_h}$ corresponding to the true phase ambiguities as follows:

$$\hat{s}_{H_k,\nabla\Delta\tilde{\mathbf{N}}^{\phi}_{WL}/H_h} = \hat{s}_{H_h,\nabla\Delta N^{\phi}_{WL}} - \mathbf{K}_{H_k}\begin{bmatrix}\mathbf{0}\\ \lambda_{WL}\varepsilon_{\nabla\Delta\tilde{\mathbf{N}}^{\phi}_{WL}}\end{bmatrix}, \quad \text{(B-10)}$$

where $\varepsilon_{\nabla\Delta\tilde{\mathbf{N}}^{\phi}_{WL}}$ is the difference between $\nabla\Delta\tilde{\mathbf{N}}^{\phi}_{WL}$ and $\nabla\Delta\mathbf{N}^{\phi}_{WL}$, namely:

$$\varepsilon_{\nabla\Delta\tilde{\mathbf{N}}^{\phi}_{WL}} = \nabla\Delta\tilde{\mathbf{N}}^{\phi}_{WL} - \nabla\Delta\mathbf{N}^{\phi}_{WL}. \quad \text{(B-11)}$$

Moreover, with the aid of Figure 2, it can be easily verified that

$$\boldsymbol{\zeta}^{(h)}_{\hat{s}_{H_h,\nabla\Delta\tilde{\mathbf{N}}^{\phi}_{WL}},\nabla\Delta\tilde{\mathbf{N}}^{\phi}_{WL}} = \boldsymbol{\zeta}^{(h)}_{\hat{s}_{H_h,\nabla\Delta N^{\phi}_{WL}},\nabla\Delta N^{\phi}_{WL}} + \boldsymbol{\Psi}_{H_k}\boldsymbol{\varepsilon}_{\nabla\Delta\tilde{\mathbf{N}}^{\phi}_{WL}}, \quad \text{(B-12)}$$

where $\boldsymbol{\Psi}_{H_k}$ is the matrix

$$\boldsymbol{\Psi}_{H_k} = -\lambda_{WL}\mathbf{C}_{\mathbf{v}_{WL}}(\mathbf{I} - \mathbf{H}_{H_k}\mathbf{G}_{H_k}\mathbf{K}_{H_k})\begin{bmatrix}\mathbf{0}\\ \mathbf{I}\end{bmatrix}. \quad \text{(B-13)}$$

Finally, by combining (B-8) and (B-12), we have:

$$\boldsymbol{\zeta}^{(h)}_{\hat{s}_{H_k,\nabla\Delta\tilde{\mathbf{N}}^{\phi}_{WL}},\nabla\Delta\tilde{\mathbf{N}}^{\phi}_{WL}} \cong \boldsymbol{\zeta}^{(h)}_{\hat{s}_{H_h,\nabla\Delta\tilde{\mathbf{N}}^{\phi}_{WL}},\nabla\Delta\mathbf{N}^{\phi}_{WL}} + \boldsymbol{\Psi}_k\boldsymbol{\varepsilon}_{\nabla\Delta\tilde{\mathbf{N}}^{\phi}_{WL}} + \boldsymbol{\Gamma}_k\mathbf{d}_{k,h}. \quad \text{(B-14)}$$

Since $\boldsymbol{\zeta}^{(h)}_{\hat{s}_{H_h,\nabla\Delta\tilde{\mathbf{N}}^{\phi}_{WL}},\nabla\Delta\mathbf{N}^{\phi}_{WL}}$ is a zero mean, Gaussian random variable with independent components, we can rotate the reference system in such a way that the first axis of the normalized residual space, say ζ_1', is parallel to $\boldsymbol{\Gamma}_k\mathbf{d}_{k,h}$, without losing independence (or changing the metric).

Then, as demonstrated in Appendix C, when

$$\left\|\left\langle \boldsymbol{\Psi}_k\boldsymbol{\varepsilon}_{\nabla\Delta\tilde{\mathbf{N}}^{\phi}_{WL}}, \frac{\boldsymbol{\Gamma}_k\mathbf{d}_{k,h}}{\|\boldsymbol{\Gamma}_k\mathbf{d}_{k,h}\|}\right\rangle\right\| \le 2\|\boldsymbol{\Gamma}_k\mathbf{d}_{k,h}\|, \quad \text{(B-15)}$$

condition $\tilde{\Lambda}^{(h)}_h > \tilde{\Lambda}^{(h)}_k$ is met almost every time when

$$\zeta_1' > -\frac{1}{2}\|\boldsymbol{\Gamma}_k\mathbf{d}_{k,h}\|. \quad \text{(B-16)}$$

Let us observe that the inter-axis between tracks is about five times the WL wavelength. Therefore, (B-15) is satisfied when only a few ambiguities around the one obtained by the MW combination are considered.

Thus, the track detector will decide on a wrong track on the left side of the true one as soon as

$$\zeta_1' < -\frac{1}{2}\|\boldsymbol{\Gamma}_{h-1}\mathbf{d}_{h-1,h}\|, \quad \text{(B-17)}$$

while it will decide on a wrong track on the right side of the true one as soon as

$$\zeta_1' < -\frac{1}{2}\|\boldsymbol{\Gamma}_{h+1}\mathbf{d}_{h+1,h}\|. \quad \text{(B-18)}$$

Considering that ζ_1' is a zero mean, Gaussian random variable with unit variance, the conditional error probability is

$$\begin{aligned} P^{\pm}_{e_h} &= \frac{1}{\sqrt{2\pi}}\int_{-\infty}^{-\frac{1}{2}\|\boldsymbol{\Gamma}_{h\pm1}\mathbf{d}_{h\pm1,h}\|} e^{-\frac{1}{2}\zeta_1'^2}d\zeta' = \\ &= \frac{1}{2}erfc\left\{\frac{\|\boldsymbol{\Gamma}_{h\pm1}\mathbf{d}_{h\pm1,h}\|}{2\sqrt{2}}\right\}, \end{aligned} \quad \text{(B-19)}$$

where $erfc(\,)$ is the complementary error function (44).

APPENDIX C. TRACK DETECTOR DECISION REGION

Assuming that the double differences of the phase ambiguities are *a priori* uniformly distributed, and observing that for a given $\boldsymbol{\varepsilon}_{\nabla\Delta\tilde{\mathbf{N}}^{\phi}_{WL}}$, both double-difference ambiguity vectors $\nabla\Delta\tilde{\mathbf{N}}^{\phi}_{WL} = \nabla\Delta\mathbf{N}^{\phi}_{WL} \pm \varepsilon_{\nabla\Delta\tilde{\mathbf{N}}^{\phi}_{WL}}$ have to be considered, we can rewrite $\tilde{\Lambda}^{(h)}_h$ and $\tilde{\Lambda}^{(h)}_k$ in condition (B-1) as follows:

$$\tilde{\Lambda}^{(h)}_h = e^{-\frac{1}{2}\|\boldsymbol{\zeta}\|^2} + \sum_{\boldsymbol{\varepsilon}_{\nabla\Delta\tilde{\mathbf{N}}^{\phi}_{WL}} \in \chi^+_{\varepsilon}} \Delta\tilde{\Lambda}^{(h)}_h\left(\boldsymbol{\varepsilon}_{\nabla\Delta\tilde{\mathbf{N}}^{\phi}_{WL}}\right), \quad \text{(C-1)}$$

$$\tilde{\Lambda}^{(h)}_k = e^{-\frac{1}{2}\|\boldsymbol{\zeta}+\boldsymbol{\Gamma}_k\mathbf{d}_{k,h}\|^2} + \sum_{\boldsymbol{\varepsilon}_{\nabla\Delta\tilde{\mathbf{N}}^{\phi}_{WL}} \in \chi^+_{\varepsilon}} \Delta\tilde{\Lambda}^{(h)}_k\left(\boldsymbol{\varepsilon}_{\nabla\Delta\tilde{\mathbf{N}}^{\phi}_{WL}}\right), \quad \text{(C-2)}$$

where

$$\begin{aligned} \Delta\tilde{\Lambda}^{(h)}_h\left(\boldsymbol{\varepsilon}_{\nabla\Delta\tilde{\mathbf{N}}^{\phi}_{WL}}\right) &= e^{-\frac{1}{2}\left\|\boldsymbol{\zeta}+\boldsymbol{\Psi}_k\boldsymbol{\varepsilon}_{\nabla\Delta\tilde{\mathbf{N}}^{\phi}_{WL}}\right\|^2} \\ &\quad + e^{-\frac{1}{2}\left\|\boldsymbol{\zeta}-\boldsymbol{\Psi}_k\boldsymbol{\varepsilon}_{\nabla\Delta\tilde{\mathbf{N}}^{\phi}_{WL}}\right\|^2}, \end{aligned} \quad \text{(C-3)}$$

$$\begin{aligned} \Delta\tilde{\Lambda}^{(h)}_k\left(\boldsymbol{\varepsilon}_{\nabla\Delta\tilde{\mathbf{N}}^{\phi}_{WL}}\right) &= e^{-\frac{1}{2}\left\|\boldsymbol{\zeta}+\boldsymbol{\Psi}_k\boldsymbol{\varepsilon}_{\nabla\Delta\tilde{\mathbf{N}}^{\phi}_{WL}}+\boldsymbol{\Gamma}_k\mathbf{d}_{k,h}\right\|^2} \\ &\quad + e^{-\frac{1}{2}\left\|\boldsymbol{\zeta}-\boldsymbol{\Psi}_k\boldsymbol{\varepsilon}_{\nabla\Delta\tilde{\mathbf{N}}^{\phi}_{WL}}+\boldsymbol{\Gamma}_k\mathbf{d}_{k,h}\right\|^2} \end{aligned} \quad \text{(C-4)}$$

and the set χ^+_{ε} is derived from $\chi_{\phi} - \left\{\nabla\Delta\mathbf{N}^{\phi}_{WL}\right\}$ by indifferently deleting either $\varepsilon_{\nabla\Delta\tilde{\mathbf{N}}^{\phi}_{WL}}$ or $-\varepsilon_{\nabla\Delta\tilde{\mathbf{N}}^{\phi}_{WL}}$.

Since $\boldsymbol{\zeta}$ is a zero mean Gaussian random variable with independent components with unit variance, any variable $\boldsymbol{\zeta}' = \mathbf{T}_{\theta}\boldsymbol{\zeta}$ obtained from $\boldsymbol{\zeta}$ by means of a

unitary matrix $\mathbf{T}_\theta$, like any combination of rotations and permutations, is still a zero mean Gaussian random variable with independent components and unit variance. Therefore, we can rotate and eventually permute ζ in such a way that the first axis of the transformed normalized residual space ζ', say ζ'_1, is parallel to $\mathbf{\Gamma}_k\mathbf{d}_{k,\,h}$, without losing independence (or changing the metric). Let

$$\mathbf{u}_{\zeta_1} = \frac{\mathbf{\Gamma}_k\mathbf{d}_{k,h}}{\left\|\mathbf{\Gamma}_k\mathbf{d}_{k,h}\right\|} \tag{C-5}$$

be the corresponding unit vector so that $\mathbf{\Gamma}_k\mathbf{d}_{k,h} = b\mathbf{u}_{\zeta_1}$, where for sake of compactness we posed

$$b = \left\|\mathbf{\Gamma}_k\mathbf{d}_{k,h}\right\|. \tag{C-6}$$

Then, with reference to the first terms of (C-1) and (C-2), we have that

$$e^{-\frac{1}{2}\|\zeta\|^2} < e^{-\frac{1}{2}\left\|\zeta+\mathbf{\Gamma}_k\mathbf{d}_{k,h}\right\|^2} \tag{C-7}$$

as soon as

$$\left\|\zeta'\right\|^2 > \left\|\zeta' + b\mathbf{u}_{\zeta'_1}\right\|^2. \tag{C-8}$$

That in turn implies

$$\zeta'_1 < -\frac{b}{2}. \tag{C-9}$$

To compare the other terms $\Delta\widetilde{\Lambda}_h^{(h)}\left(\underset{\nabla\Delta\mathbf{N}_{WL}}{\boldsymbol{\varepsilon}^{\sim\phi}}\right)$ and $\Delta\widetilde{\Lambda}_k^{(h)}\left(\underset{\nabla\Delta\mathbf{N}_{WL}}{\boldsymbol{\varepsilon}^{\sim\phi}}\right)$ of (C-1) and (C-2), for a given $\mathbf{\Psi}_k\underset{\nabla\Delta\mathbf{N}_{WL}}{\boldsymbol{\varepsilon}^{\sim\phi}}$, let us consider the transformation $\mathbf{T}_\theta$ such that the second component ζ'_2 of ζ' is coplanar with $\mathbf{\Psi}_k\underset{\nabla\Delta\mathbf{N}_{WL}}{\boldsymbol{\varepsilon}^{\sim\phi}}$ and $\mathbf{\Gamma}_k\mathbf{d}_{k,h}$ and orthogonal to ζ'_1, and let $\mathbf{u}_{\zeta_2}$ be the corresponding unit vector.

For sake of compactness let us pose in the following:

$$a_1 = \mathbf{\Psi}_k\underset{\nabla\Delta\mathbf{N}_{WL}}{\boldsymbol{\varepsilon}^{\sim\phi}}, \mathbf{u}_{\zeta_1}, \tag{C-10}$$

$$a_2 = \mathbf{\Psi}_k\underset{\nabla\Delta\mathbf{N}_{WL}}{\boldsymbol{\varepsilon}^{\sim\phi}}, \mathbf{u}_{\zeta_2}, \tag{C-11}$$

so that

$$\mathbf{\Psi}_k\underset{\nabla\Delta\mathbf{N}_{WL}}{\boldsymbol{\varepsilon}^{\sim\phi}} = a_1\mathbf{u}_{\zeta_1} + a_1\mathbf{u}_{\zeta_2}. \tag{C-12}$$

Moreover, with reference to Figure 15, let us introduce the vectors $\mathbf{s}_1$, $\mathbf{s}_2$,$\mathbf{v}_1$, and$\mathbf{v}_2$ defined as in Table 2.

The comparison among the norms of $\mathbf{s}_1$, $\mathbf{s}_2$, $\mathbf{v}_1$, and $\mathbf{v}_2$ is reported in Table 2 and in Table 3.

From Table 2, it follows that a sufficient condition for which $\Delta\widetilde{\Lambda}_h^{(h)}\left(\underset{\nabla\Delta\mathbf{N}_{WL}}{\boldsymbol{\varepsilon}^{\sim\phi}}\right) > \Delta\widetilde{\Lambda}_k^{(h)}\left(\underset{\nabla\Delta\mathbf{N}_{WL}}{\boldsymbol{\varepsilon}^{\sim\phi}}\right)$ is that either

$$\|\mathbf{v}_1\|^2 > \|\mathbf{s}_1\|^2 and \|\mathbf{v}_2\|^2 > \|\mathbf{s}_2\|^2 \tag{C-13}$$

or

$$\|\mathbf{v}_1\|^2 > \|\mathbf{s}_2\|^2 and \|\mathbf{v}_2\|^2 > \|\mathbf{s}_1\|^2 \tag{C-14}$$

or

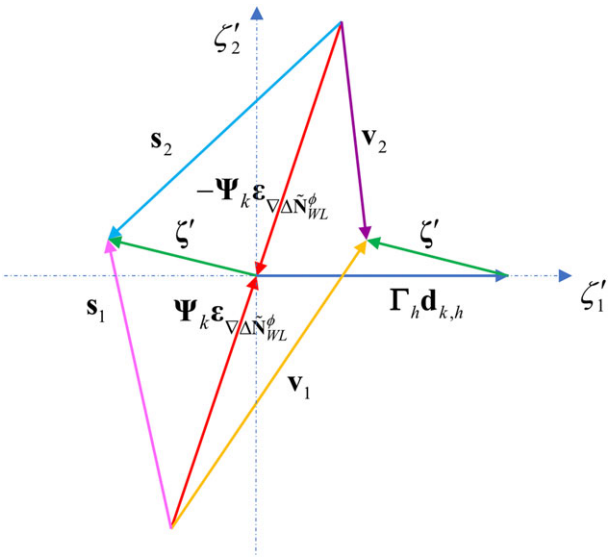

Fig. 15–Normalized residual space geometry. [Color figure can be viewed at wileyonlinelibrary.com and www.ion.org]

Table 2—Vector definitions

Vector	Components
$\mathbf{s}_1 = \zeta + \mathbf{\Psi}_k\underset{\nabla\Delta\mathbf{N}_{WL}}{\boldsymbol{\varepsilon}^{\sim\phi}}$	$\mathbf{s}_1 = \begin{bmatrix}\zeta'_1 + a_1 & \zeta'_2 + a_2\end{bmatrix}$
$\mathbf{s}_2 = \zeta - \mathbf{\Psi}_k\underset{\nabla\Delta\mathbf{N}_{WL}}{\boldsymbol{\varepsilon}^{\sim\phi}}$	$\mathbf{s}_2 = \begin{bmatrix}\zeta'_1 - a_1 & \zeta'_2 - a_2\end{bmatrix}$
$\mathbf{v}_1 = \zeta + \mathbf{\Psi}_k\underset{\nabla\Delta\mathbf{N}_{WL}}{\boldsymbol{\varepsilon}^{\sim\phi}} + \mathbf{\Gamma}_k\mathbf{d}_{k,h}$	$\mathbf{v}_1 = \begin{bmatrix}\zeta'_1 + a_1 + b & \zeta'_2 + a_2\end{bmatrix}$
$\mathbf{v}_2 = \zeta - \mathbf{\Psi}_k\underset{\nabla\Delta\mathbf{N}_{WL}}{\boldsymbol{\varepsilon}^{\sim\phi}} + \mathbf{\Gamma}_k\mathbf{d}_{k,h}$	$\mathbf{v}_2 = \begin{bmatrix}\zeta'_1 - a_1 + b & \zeta'_2 - a_2\end{bmatrix}$

Table 3—Norm comparison

	$\leq\|\mathbf{s}_1\|^2$	$\leq\|\mathbf{s}_2\|^2$
$\|\mathbf{v}_1\|^2$	$\zeta'_1 < -\frac{b}{2} - a_1$	$\zeta'_1 < -\frac{b}{2} - \frac{2a_2}{b+2a_1}\zeta'_2$
$\|\mathbf{v}_2\|^2$	(1) $b > 2a_1$	$\zeta'_1 < -\frac{b}{2} + a_1$
	$\zeta'_1 < -\frac{b}{2} + \frac{2a_2}{b-2a_1}\zeta'_2$	
	(2) $b < 2a_1$	
	$\zeta'_1 > -\frac{b}{2} + \frac{2a_2}{b-2a_1}\zeta'_2$	

$$\min\left\{\|\mathbf{v}_1\|^2, \|\mathbf{v}_2\|^2\right\} > \|\mathbf{s}_1\|^2 + \ln 4. \tag{C-15}$$

For the last condition, observe that

$$e^{-\frac{1}{2}\|\mathbf{s}_1\|^2} + e^{-\frac{1}{2}\|\mathbf{s}_2\|^2} > e^{-\frac{1}{2}\|\mathbf{s}_1\|^2}, \tag{C-16}$$

and

$$2e^{-\frac{1}{2}\min\left\{\|\mathbf{v}_1\|^2,\|\mathbf{v}_2\|^2\right\}} \geq e^{-\frac{1}{2}\|\mathbf{v}_1\|^2} + e^{-\frac{1}{2}\|\mathbf{v}_2\|^2}. \tag{C-17}$$

Therefore, when condition (C-15) holds, we have that

$$e^{-\frac{1}{2}\|\mathbf{s}_1\|^2} > 2e^{-\frac{1}{2}\min\left\{\|\mathbf{v}_1\|^2,\|\mathbf{v}_2\|^2\right\}} \tag{C-18}$$

so that $\Delta\widetilde{\Lambda}_h^{(h)}\left(\underset{\nabla\Delta\mathbf{N}_{WL}}{\boldsymbol{\varepsilon}^{\sim\phi}}\right) > \Delta\widetilde{\Lambda}_k^{(h)}\left(\underset{\nabla\Delta\mathbf{N}_{WL}}{\boldsymbol{\varepsilon}^{\sim\phi}}\right)$.

Table 4—Sets for which $\Delta\widetilde{\Lambda}_h^{(h)}\left(\underset{\nabla\Delta\mathbf{N}_{WL}}{\boldsymbol{\varepsilon}}^{\phi}\right) > \Delta\widetilde{\Lambda}_k^{(h)}\left(\underset{\nabla\Delta\mathbf{N}_{WL}}{\boldsymbol{\varepsilon}}^{\phi}\right)$ and $e^{-\frac{1}{2}\|\zeta\|^2} > e^{-\frac{1}{2}\left\|\zeta+\Gamma_k\mathbf{d}_{k,h}\right\|^2}$

Id	Property	Set
Φ_1	$\|\mathbf{v}_1\|^2 > \|\mathbf{s}_1\|^2$and $\|\mathbf{v}_2\|^2 > \|\mathbf{s}_2\|^2$	$\left\{\zeta'_1 > -\frac{b}{2}+a_1\right\}$
Φ_2	$\|\mathbf{v}_1\|^2 > \|\mathbf{s}_2\|^2$and $\|\mathbf{v}_2\|^2 > \|\mathbf{s}_1\|^2$	$\left\{\zeta'_1 > -\frac{b}{2}-\frac{2a_2}{b+2a_1}\zeta'_2\right\}\cap \left\{\zeta'_1 > -\frac{b}{2}+\frac{2a_2}{b-2a_1}\zeta'_2\right\}$
Φ_3	$\|\mathbf{v}_1\|^2 = \min\left\{\|\mathbf{v}_1\|^2, \|\mathbf{v}_2\|^2\right\}$ and $\|\mathbf{v}_1\|^2 > \|\mathbf{s}_1\|^2 + \ln 4$	$\left\{\zeta'_1 < -\frac{a_2}{a_1}\zeta'_2\right\}\cap\left\{\zeta'_1 < -\frac{b}{2}\right\}\cap \left\{\zeta'_1 > -\frac{b}{2}-a_1+\frac{\ln 2}{b}\right\}$
Φ_4	$\|\mathbf{v}_2\|^2 = \min\left\{\|\mathbf{v}_1\|^2, \|\mathbf{v}_2\|^2\right\}$ and $\|\mathbf{v}_2\|^2 > \|\mathbf{s}_1\|^2 + \ln 4$	$\left\{\zeta'_1 > -\frac{a_2}{a_1}\zeta'_2\right\}\cap\left\{\zeta'_1 < -\frac{b}{2}\right\}\cap \left\{\zeta'_1 > -\frac{b}{2}+\frac{4a_2\zeta'_2-\ln 2}{b-2a_1}\right\}$

The sets and corresponding to sufficient conditions (C-13), (C-14), and (C-15) are reported in Table 4.

Similarly, a sufficient condition for which $\Delta\widetilde{\Lambda}_h^{(h)}\left(\underset{\nabla\Delta\mathbf{N}_{WL}}{\boldsymbol{\varepsilon}}^{\phi}\right) < \Delta\widetilde{\Lambda}_k^{(h)}\left(\underset{\nabla\Delta\mathbf{N}_{WL}}{\boldsymbol{\varepsilon}}^{\phi}\right)$ is that either

$$\|\mathbf{v}_1\|^2 < \|\mathbf{s}_1\|^2 \, and \, \|\mathbf{v}_2\|^2 < \|\mathbf{s}_2\|^2 \tag{C-19}$$

or

$$\|\mathbf{v}_1\|^2 \leq \|\mathbf{s}_2\|^2 \, and \, \|\mathbf{v}_2\|^2 \leq \|\mathbf{s}_1\|^2 \tag{C-20}$$

$$\min\left\{\|\mathbf{s}_1\|^2, \|\mathbf{s}_2\|^2\right\} > \|\mathbf{v}_2\|^2 + \ln 4. \tag{C-21}$$

The sets corresponding to sufficient conditions (C-19), (C-20), and (C-21) for the case $b > 2a_1$ are reported in Table 5.

Table 5—Sets for which $\Delta\widetilde{\Lambda}_h^{(h)}\left(\underset{\nabla\Delta\mathbf{N}_{WL}}{\boldsymbol{\varepsilon}}^{\phi}\right) < \Delta\widetilde{\Lambda}_k^{(h)}\left(\underset{\nabla\Delta\mathbf{N}_{WL}}{\boldsymbol{\varepsilon}}^{\phi}\right)$ and $e^{-\frac{1}{2}\|\zeta\|^2} < e^{-\frac{1}{2}\left\|\zeta+\Gamma_k\mathbf{d}_{k,h}\right\|^2}$

Id	Property	Set
Ω_1	$\|\mathbf{v}_1\|^2 < \|\mathbf{s}_1\|^2$and $\|\mathbf{v}_2\|^2 < \|\mathbf{s}_2\|^2$	$\left\{\zeta'_1 < -\frac{b}{2}-a_1\right\}$
Ω_2	$\|\mathbf{v}_1\|^2 \leq \|\mathbf{s}_2\|^2$and $\|\mathbf{v}_2\|^2 \leq \|\mathbf{s}_1\|^2$	$\left\{\zeta'_1 < -\frac{b}{2}-\frac{2a_2}{b+2a_1}\zeta'_2\right\}\cap \left\{\zeta'_1 < -\frac{b}{2}+\frac{2a_2}{b-2a_1}\zeta'_2\right\}$
Ω_3	$\|\mathbf{s}_2\|^2 = \min\left\{\|\mathbf{s}_1\|^2, \|\mathbf{s}_2\|^2\right\}$ and $\|\mathbf{s}_2\|^2 > \|\mathbf{v}_2\|^2 + \ln 4$	$\left\{\zeta'_1 > -\frac{a_2}{a_1}\zeta'_2\right\}\cap\left\{\zeta'_1 > -\frac{b}{2}\right\}\cap \left\{\zeta'_1 < -\frac{b}{2}+a_1-\frac{\ln 2}{b}\right\}$
Ω_4	$\|\mathbf{s}_1\|^2 = \min\left\{\|\mathbf{s}_1\|^2, \|\mathbf{s}_2\|^2\right\}$ and $\|\mathbf{s}_1\|^2 > \|\mathbf{v}_2\|^2 + \ln 4$	$\left\{\zeta'_1 < -\frac{a_2}{a_1}\zeta'_2\right\}\cap\left\{\zeta'_1 > -\frac{b}{2}\right\}\cap \left\{\zeta'_1 > -\frac{b}{2}+\frac{4a_2\zeta'_2+\ln 2}{b-2a_1}\right\}$

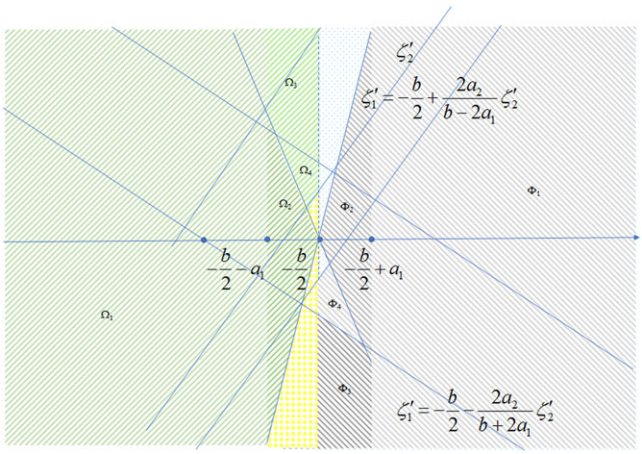

Fig. 16–Decision regions analysis. The area with a +45 degrees hatched pattern correspond to Ω_1, Ω_2, Ω_3, Ω_4. The area with a −45 degrees hatched pattern correspond to Φ_1, Φ_2, Φ_3, Φ_4. [Color figure can be viewed at wileyonlinelibrary.com and www.ion.org]

In Figure 16, the regions for which those sufficient conditions for $\Delta\widetilde{\Lambda}_h^{(h)}\left(\underset{\nabla\Delta\mathbf{N}_{WL}}{\boldsymbol{\varepsilon}}^{\phi}\right) > \Delta\widetilde{\Lambda}_k^{(h)}\left(\underset{\nabla\Delta\mathbf{N}_{WL}}{\boldsymbol{\varepsilon}}^{\phi}\right)$ hold are filled with a −45 degrees hatched pattern, while the regions for which those sufficient conditions for $\Delta\widetilde{\Lambda}_h^{(h)}\left(\underset{\nabla\Delta\mathbf{N}_{WL}}{\boldsymbol{\varepsilon}}^{\phi}\right) < \Delta\widetilde{\Lambda}_k^{(h)}\left(\underset{\nabla\Delta\mathbf{N}_{WL}}{\boldsymbol{\varepsilon}}^{\phi}\right)$ and $e^{-\frac{1}{2}\|\zeta\|^2} > e^{-\frac{1}{2}\left\|\zeta+\Gamma_k\mathbf{d}_{k,h}\right\|^2}$ hold are filled with a +45 degrees hatched pattern. The region for which only $e^{-\frac{1}{2}\|\zeta\|^2} > e^{-\frac{1}{2}\left\|\zeta+\Gamma_k\mathbf{d}_{k,h}\right\|^2}$ holds is filled in cyan, while the region for which only $e^{-\frac{1}{2}\|\zeta\|^2} < e^{-\frac{1}{2}\left\|\zeta+\Gamma_k\mathbf{d}_{k,h}\right\|^2}$ holds is filled in yellow.

We finally observe that

$$P_\Phi \leq \text{Prob}\left\{\widetilde{\Lambda}_k^{(h)} > \widetilde{\Lambda}_h^{(h)}\right\} \leq 1 - P_\Omega, \tag{C-22}$$

where

$$\mathrm{P}_\Phi = \frac{1}{2\pi}\iint_\Phi \exp\left\{-\frac{\zeta'^2_1+\zeta'^2_2}{2}\right\} d\zeta'_1 d\zeta'_2, \tag{C-23}$$

with $\Phi = \Phi_1 \cup \Phi_2 \cup \Phi_3 \cup \Phi_4$ and

$$\mathrm{P}_\Omega = \frac{1}{2\pi}\iint_\Omega \exp\left\{-\frac{\zeta'^2_1+\zeta'^2_2}{2}\right\} d\zeta'_1 d\zeta'_2, \tag{C-24}$$

with $\Omega = \Omega_1 \cup \Omega_2 \cup \Omega_3 \cup \Omega_4$.

Considering that $\widetilde{\Lambda}_h^{(h)}$ and $\widetilde{\Lambda}_k^{(h)}$ are essentially approximated by the first term, based on (C-22), we approximate $\text{Prob}\left\{\widetilde{\Lambda}_k^{(h)} > \widetilde{\Lambda}_h^{(h)}\right\}$ as

$$\text{Prob}\left\{\widetilde{\Lambda}_k^{(h)} > \widetilde{\Lambda}_h^{(h)}\right\} \cong \frac{1}{2\pi}\int_{-\infty}^{-\frac{b}{2}}\int_{-\infty}^{+\infty} \exp\left\{-\frac{\zeta'^2_1+\zeta'^2_2}{2}\right\} d\zeta' \, d\zeta'_2 = \\ = \frac{1}{2} erfc\left\{\frac{b}{2\sqrt{2}}\right\}. \tag{C-25}$$

ACKNOWLEDGMENTS

This work has been developed under the grant of the "RHINOS" project of the H2020-Galileo-GSA-2014-2015/H2020-Galileo-2015-1 Program (project number 687399).

REFERENCES

1. Neri, A., Rispoli, F., and Salvatori, P., "The Perspective of Adopting the GNSS for the Evolution of the European Train Control System (ERTMS): A Roadmap for Standardized and Certifiable Platform," *Proceedings of the 28th International Technical Meeting of the Satellite Division of The Institute of Navigation (ION GNSS+ 2015)*, Tampa, FL, September 2015, pp. 542-552.
2. Neri, A., Rispoli, F., and Salvatori, P., "A GNSS Based Solution for Supporting Virtual Block Operations in Train Control Systems," *IAIN-2015*, Prague, Czech Republic, 2015.
3. Neri, A., Sabina, S., and Mascia, U., "GNSS and Odometry Fusion for High Integrity and High Available Train Control Systems," *Proceedings of the 28th International Technical Meeting of the Satellite Division of The Institute of Navigation (ION GNSS+ 2015*), Tampa, FL, September 2015, pp. 639-648.
4. Neri, A., Vegni, A. M., and Rispoli, F., "A PVT Estimation for the ERTMS Train Control Systems in Presence of Multiple Tracks," *Proceedings of the 26th International Technical Meeting of the Satellite Division of The Institute of Navigation (ION GNSS 2013),* Nashville, TN, September 2013, pp. 631-644.
5. Teunissen, P. J. G., de Jonge, P. J., and Tiberius, C. C. J. M., "The LAMBDA Method for Fast GPS Surveying," *Proceedings of International Symposium on GPS Technology Applications*, 1995.
6. Chang, X. W., Yang, X., and Zhou, T., "MLAMBDA: A Modified LAMBDA Method for Integer Least-Squares Estimation," *Journal of Geodesy*, December 2005.
7. Liu, J., Cannon, M. E., Alves, P., Petovello, M. G., Lachapelle, G., MacGougan, G., and DeGroot, L., "A Performance Comparison of Single and Dual (C-26) Frequency GPS Ambiguity Resolution Strategies," *GPS Solutions*, 2003.
8. Verhagen, S., Teunissen, P. J.G., van der Marel, H., and Li, B., "GNSS Ambiguity Resolution: Which Subset to Fix?" *International Global Navigation Satellite Systems Society (IGNSS) Symposium*, 2011.
9. Mowlam, A., "Baseline Precision Results Using Triple Frequency Partial Ambiguity Sets," *Proceedings of the 17th International Technical Meeting of the Satellite Division of The Institute of Navigation (ION GNSS 2004)*, Long Beach, CA, September 2004, pp. 2509-2518.
10. Cao, W., O'Keefe, K., and Cannon, M. E., "Partial Ambiguity Fixing within Multiple Frequencies and Systems," *Proceedings of the 20th International Technical Meeting of the Satellite Division of The Institute of Navigation (ION GNSS 2007)*, Fort Worth, TX, September 2007, pp. 312-323.
11. Feng, Y. and Wang, J., "GPS RTK Performance Characteristics and Analysis," *The Journal of Global Positioning Systems*, Vol. 7, No. 1, 2008, pp. 1-8.
12. Hu, G. R., Khoo, H. S., Goh, P. C., and Law, C. L., "Development and Assessment of GPS Virtual Reference Stations for RTK Positioning," *Journal of Geodesy*, Vol. 77, 2003, pp. 292–302.
13. Li, S., Wang, Y., and Han, Y., "Summary of Network RTK Reference Station Ambiguity Determination," *2010 6th International Conference on Wireless Communications Networking and Mobile Computing (WiCOM)*, Chengdu, 2010, pp. 1-5.
14. Van Trees, *Detection, Estimation, and Modulation Theory, Part III*, New York: John Wiley & Sons, 2001, p. 237.
15. Helstrom, C. W., *Statistical Theory of Signal Detection*, Pergamon, 1960, pp. 248-249.
16. Van Trees, *Detection, Estimation, and Modulation Theory, Part I*, New York: John Wiley & Sons, 2001, pp. 92-93.
17. Neri, A., Rispoli, F., and Salvatori, P., "CENELEC SIL-4 Compliant Approach for Discriminating Railway Parallel Tracks Based on EGNOS-GALILEO Receivers," *ENC-GNSS 2014*, April 2014.
18. Neri, A., Palma, V., Rispoli, F., and Vegni, A. M., "Track Constrained PVT Estimation Based on the Double-Difference Technique for Railway Applications," *Proceedings of EUSIPCO 2013*, Marrakech, Morocco, September 2013.
19. Sanz Subirana, J., Juan Zornoza, J. M., and Hernández-Pajares, M., *GNSS Data Processing Volume I: Fundamentals and Algorithms*, ESA TM-23/1, May 2013.